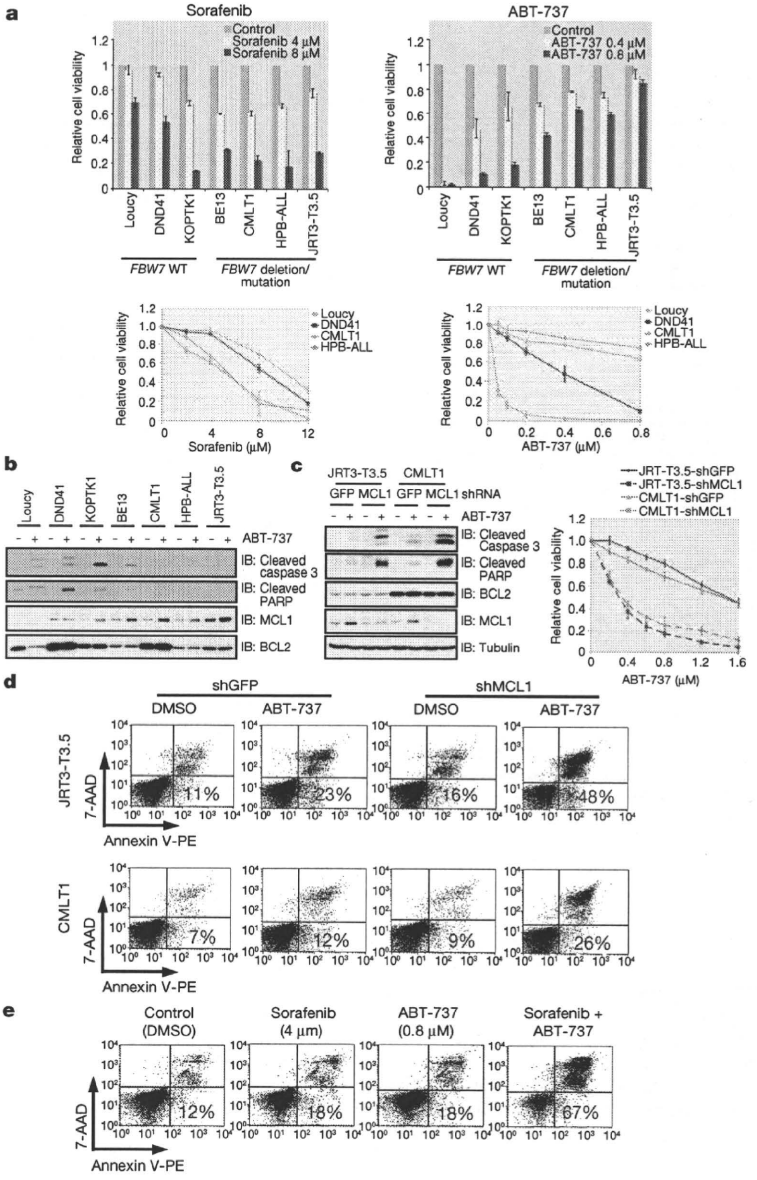


**Figure 4 | Elevated MCL1 expression protects FBW7-deficient T-ALL cell lines from ABT-737-induced apoptosis. a**, Cell viability assays showing that FBW7-deficient human T-ALL cell lines were more sensitive to sorafenib but were relatively resistant to ABT-737 treatment. T-ALL cells were cultured in 10% FBS-containing medium with the indicated concentrations of sorafenib or ABT-737 for 48 h before cell viability assays were performed. Data are shown as mean ± s.d. for three independent experiments. **b**, IB analysis of the indicated human T-ALL cell lines with or without ABT-737 (0.8 μM) treatment. PARP, poly(ADP-ribose) polymerase. **c**, Specific depletion of endogenous MCL1 expression restored sensitivity to ABT-737 in the indicated FBW7-deficient human T-ALL cell lines. Various T-ALL cell lines were infected with lentiviral shGFP- or shMCL1-encoding vectors and selected in 0.5 μg ml$^{-1}$ puromycin to eliminate non-infected cells. The generated cell lines were cultured in 10% FBS-containing medium with the indicated concentrations of ABT-737 for 48 h before cell viability assays were performed (right) or with or without ABT-737 (0.8 μM) treatment for 24 h before WCL were collected for IB analysis with antibodies specific for the indicated proteins (left). For cell viability assays, data are shown as mean ± s.d. for three independent experiments. **d**, Double staining with 7-AAD and annexin-V–PE (annexin V conjugated to phycoerythrin), followed by flow cytometry analysis to detect the percentage of apoptotic cells (axes indicate intensity of fluorochrome). In the indicated FBW7-deficient human T-ALL cell lines, endogenous MCL1 was depleted by infection with lentiviral vectors encoding shRNA (lentiviral shGFP was used as a negative control). Cell lines were cultured in 10% FBS-containing medium with or without ABT-737 (0.8 μM) treatment, with DMSO as a negative control, for 48 h before the flow cytometry analysis. Purple numbers indicate the percentage of apoptotic cells. **e**, Staining and flow cytometry analysis as in **d**, demonstrating that sorafenib treatment restores ABT-737 sensitivity to FBW7-deficient HPB-ALL cells. HPB-ALL cells were cultured in 10% FBS-containing medium with the indicated concentrations of sorafenib and/or ABT-737 for 48 h before analysis. Coloured numbers indicate the percentage of apoptotic cells.

the primary cause of desensitization to ABT-737 *in vivo*[23,24]. It also suggests that patients with FBW7-deficient T-ALL will not respond well to treatment with ABT-737. We further demonstrated that manipulation of FBW7 activity or ectopic expression of a non-degradable form of MCL1 in human T-ALL cells affects their sensitivity to ABT-737 (Supplementary Fig. 10a, b) and responses to other apoptotic stimuli (Supplementary Fig. 10c–f).

Our results indicate that inhibition of MCL1 could be used to restore sensitivity to ABT-737 in FBW7-deficient T-ALL cells. Given that the clinical application of siRNA- or short hairpin RNA (shRNA)-mediated target extinction is not yet feasible owing to delivery challenges, we instead exploited small molecule strategies to reduce MCL1 expression, specifically with the use of sorafenib (Supplementary Fig. 9h). The combined use of sorafenib and ABT-737 produced a dose-dependent

increase in the sensitivity of HPB-ALL cells, a human T-ALL cell line, to ABT-737 (Supplementary Fig. 10g), and this decrease correlated with a significant increase in the induction of apoptosis (Fig. 4e). Similar results were obtained for other FBW7-deficient T-ALL cell lines (Supplementary Fig. 10h).

Our studies provide experimental evidence of a role for FBW7 in governing the apoptotic pathway by controlling MCL1 destruction. MCL1 has a key role in regulating the apoptosis of T cells[14] but not of cells from other tissue types, such as liver cells. Therefore, our studies also provide a possible mechanistic explanation for why loss of *FBW7* is frequently seen in patients with T-ALL. Although other E3 ubiquitin ligases, including MULE[25] and β-transducin-repeat-containing protein (β-TRCP)[17], have been implicated in controlling MCL1 stability, MULE activity was not implicated in the GSK3-dependent regulation of MCL1 (refs 17, 25) (Supplementary Fig. 11a–e). Additionally, no correlation was found between MULE and MCL1 expression in various T-ALL cells (Supplementary Fig. 11f), thereby excluding a physiological role for MULE in regulating MCL1 abundance in T-ALL cells. We further found that depletion of FBW7, but not β-TRCP, leads to a significant induction of MCL1 expression (Fig. 1b and Supplementary Fig. 11a–c). Array comparative genomic hybridization analysis demonstrated a high frequency of *FBW7* loss[2] but not simultaneous loss of *BTRC1* and *BTRC2*, which encode β-TRCPs, in T-ALL cells (data not shown). Together, these data support the hypothesis that $SCF^{FBW7}$ is a physiological E3 ubiquitin ligase for MCL1, with USP9X being the nominated deubiquitylase[26], and that loss of *FBW7* contributes to T-ALL development through the upregulation of MCL1 expression. More importantly, our studies suggest that there is a correlation between *FBW7* genetic status and sensitivity to ABT-737, and they provide insight into the use of MCL1 inhibitors as a practical method for specifically killing FBW7-deficient T-ALL cells. This work provides a basis for the rational treatment of patients with T-ALL and provides motivation for the development of specific MCL1 antagonists, or agents that significantly reduce MCL1 expression, for the improved management of patients with T-ALL.

## METHODS SUMMARY

Expression plasmid constructs, proteins, antibodies and cell lines are described in the Methods. The sequences of various siRNA oligonucleotides used in this study are also listed in the Methods. *In vivo* phosphorylation of MCL1 was detected by mass spectrometry analysis, and the major GSK3-dependent phosphorylation sites that were identified were subsequently examined by *in vitro* kinase assays. All mutants were generated using PCR, and the sequences were verified. FBW7-mediated MCL1 ubiquitylation and destruction were examined by cell-based ubiquitylation and degradation assays. Cell viability assays were used to detect the response of various T-ALL cell lines to sorafenib and ABT-737. Double staining with annexin V and 7-AAD was used to detect the percentage of apoptotic cells.

**Full Methods** and any associated references are available in the online version of the paper at www.nature.com/nature.

**Received 12 October 2009; accepted 29 November 2010.**


1. Wood, L. D. *et al.* The genomic landscapes of human breast and colorectal cancers. *Science* **318,** 1108–1113 (2007).
2. Maser, R. S. *et al.* Chromosomally unstable mouse tumours have genomic alterations similar to diverse human cancers. *Nature* **447,** 966–971 (2007).
3. Onoyama, I. *et al.* Conditional inactivation of *Fbxw7* impairs cell-cycle exit during T cell differentiation and results in lymphomatogenesis. *J. Exp. Med.* **204,** 2875–2888 (2007).
4. Matsuoka, S. *et al.* Fbxw7 acts as a critical fail-safe against premature loss of hematopoietic stem cells and development of T-ALL. *Genes Dev.* **22,** 986–991 (2008).
5. Thompson, B. J. *et al.* The $SCF^{FBW7}$ ubiquitin ligase complex as a tumor suppressor in T cell leukemia. *J. Exp. Med.* **204,** 1825–1835 (2007).
6. Wei, W., Jin, J., Schlisio, S., Harper, J. W. & Kaelin, W. G. Jr. The v-Jun point mutation allows c-Jun to escape GSK3-dependent recognition and destruction by the Fbw7 ubiquitin ligase. *Cancer Cell* **8,** 25–33 (2005).
7. Welcker, M. *et al.* The Fbw7 tumor suppressor regulates glycogen synthase kinase 3 phosphorylation-dependent c-Myc protein degradation. *Proc. Natl Acad. Sci. USA* **101,** 9085–9090 (2004).
8. Koepp, D. M. *et al.* Phosphorylation-dependent ubiquitination of cyclin E by the $SCF^{Fbw7}$ ubiquitin ligase. *Science* **294,** 173–177 (2001).
9. Gupta-Rossi, N. *et al.* Functional interaction between SEL-10, an F-box protein, and the nuclear form of activated Notch1 receptor. *J. Biol. Chem.* **276,** 34371–34378 (2001).
10. Shaulian, E. & Karin, M. AP-1 as a regulator of cell life and death. *Nature Cell Biol.* **4,** E131–E136 (2002).
11. Sanchez, I. & Yuan, J. A convoluted way to die. *Neuron* **29,** 563–566 (2001).
12. Akgul, C. Mcl-1 is a potential therapeutic target in multiple types of cancer. *Cell. Mol. Life Sci.* **66,** 1326–1336 (2009).
13. Maurer, U., Charvet, C., Wagman, A. S., Dejardin, E. & Green, D. R. Glycogen synthase kinase-3 regulates mitochondrial outer membrane permeabilization and apoptosis by destabilization of MCL-1. *Mol. Cell* **21,** 749–760 (2006).
14. Opferman, J. T. *et al.* Development and maintenance of B and T lymphocytes requires antiapoptotic MCL-1. *Nature* **426,** 671–676 (2003).
15. Wertz, I. E. *et al.* Sensitivity to antitubulin chemotherapeutics is regulated by MCL1 and FBW7. *Nature* doi:10.1038/nature09779 (this issue).
16. Welcker, M. & Clurman, B. E. FBW7 ubiquitin ligase: a tumour suppressor at the crossroads of cell division, growth and differentiation. *Nature Rev. Cancer* **8,** 83–93 (2008).
17. Ding, Q. *et al.* Degradation of Mcl-1 by β-TrCP mediates glycogen synthase kinase 3-induced tumor suppression and chemosensitization. *Mol. Cell. Biol.* **27,** 4006–4017 (2007).
18. Nijhawan, D. *et al.* Elimination of Mcl-1 is required for the initiation of apoptosis following ultraviolet irradiation. *Genes Dev.* **17,** 1475–1486 (2003).
19. Panka, D. J., Cho, D. C., Atkins, M. B. & Mier, J. W. GSK-3β inhibition enhances sorafenib-induced apoptosis in melanoma cell lines. *J. Biol. Chem.* **283,** 726–732 (2008).
20. Yu, C. *et al.* The role of Mcl-1 downregulation in the proapoptotic activity of the multikinase inhibitor BAY 43-9006. *Oncogene* **24,** 6861–6869 (2005).
21. Sharma, S. V. & Settleman, J. Oncogene addiction: setting the stage for molecularly targeted cancer therapy. *Genes Dev.* **21,** 3214–3231 (2007).
22. Cragg, M. S., Harris, C., Strasser, A. & Scott, C. L. Unleashing the power of inhibitors of oncogenic kinases through BH3 mimetics. *Nature Rev. Cancer* **9,** 321–326 (2009).
23. Konopleva, M. *et al.* Mechanisms of antileukemic activity of the novel Bcl-2 homology domain-3 mimetic GX15-070 (obatoclax). *Cancer Res.* **68,** 3413–3420 (2008).
24. van Delft, M. F. *et al.* The BH3 mimetic ABT-737 targets selective Bcl-2 proteins and efficiently induces apoptosis via Bak/Bax if Mcl-1 is neutralized. *Cancer Cell* **10,** 389–399 (2006).
25. Zhong, Q., Gao, W., Du, F. & Wang, X. Mule/ARF-BP1, a BH3-only E3 ubiquitin ligase, catalyzes the polyubiquitination of Mcl-1 and regulates apoptosis. *Cell* **121,** 1085–1095 (2005).
26. Schwickart, M. *et al.* Deubiquitinase USP9X stabilizes MCL1 and promotes tumour cell survival. *Nature* **463,** 103–107 (2010).


**Supplementary Information** is linked to the online version of the paper at www.nature.com/nature.

**Acknowledgements** We thank J. Lawler, C. Schorl, Q. Zhang and S. Glueck for critical reading of the manuscript, J. DeCaprio, M.-C. Hung, M. A. Kelliher, W. Harper and W. Hahn for providing reagents, L. Cantley and A. Toker for suggestions, I. Wertz and V. Dixit for sharing unpublished data, and members of the Wei and DePinho labs for useful discussions. W.W. is a Kimmel Scholar and V Scholar. This work was supported in part by the Emerald Foundation New Investigator award (W.W.), the Leukemia and Lymphoma Society Special Fellow award (W.W.) and a grant from the National Institutes of Health (W.W.; GM089763). R.A.D. is an American Cancer Society Research Professor and is supported by the Robert A. and Renée E. Belfer Foundation Institute for Applied Cancer Science.

**Author Contributions** H.I. performed most of the experiments with critical assistance from S.S. and D.G. A.T., L.W. and A.W.L. also helped perform a portion of the experiments. I.O. performed the *Fbw7* conditional knockout mouse experiments, and A.L.C. performed the orthotopic engraftment mouse experiments. B.Z. performed the mass spectrometry analysis, and Y.X. and R.S.M. helped to perform the experiments with tumours derived from the TKO mice. A.G. helped to perform the experiments with the human T-ALL clinical samples. W.W., R.A.D. and K.I.N. designed the experiments with assistance from J.A., J. S., A.L.K., H.I., S.P.G. and T.L. W.W. supervised the study. W.W. wrote the manuscript with help from H.I. and S.S. All authors commented on the manuscript.

**Author Information** Reprints and permissions information is available at www.nature.com/reprints. The authors declare no competing financial interests. Readers are welcome to comment on the online version of this article at www.nature.com/nature. Correspondence and requests for materials should be addressed to W.W. (wwei2@bidmc.harvard.edu).

## METHODS

**Plasmids.** HA–FBW7 and HA–GSK3 constructs were described previously[6]. Human *FBW7* cDNA was subcloned using Pfu polymerase (Stratagene) into the pBabe-Puro-HA retrovirus vector. Myc–MCL1 WT, Myc–MCL1 3A, and GST–MCL1 WT constructs were gifts from M.-C. Hung. FBW7 and MCL1 mutants were generated with the QuikChange XL Site-Directed Mutagenesis Kit (Stratagene) according to the manufacturer's instructions. HA–ERK1, shERK1 and shERK2 constructs were gifts from J. Blenis. Flag–β-TRCP1, Flag–Ub, shTRCP1 and shTRCP1+2 retroviral constructs were gifts from W. Harper. The shFBW7 retroviral vector (Addgene) was validated and described previously[27]. To generate the lentiviral shFBW7 and shMULE vectors, DNA oligonucleotides encoding shRNA directed against FBW7 and MULE were annealed and subcloned into AgeI and EcoRI sites of the pLKO lentiviral plasmid. The following are DNA oligonucleotide sequences for the *FBW7*-directed shRNA (sense, 5′-CCGGAACCTTCTCTGGAGAGAGAAACTCGAGTTTCTCTCTCCAGAGAAGGTTTTTTTG-3′; antisense, 5′-AATTCAAAAAAACCTTCTCTGGAGAGAGAAACTCGAGTTTCTCTCTCCAGAGAAGGTT-3′), and for MULE-directed shRNA (sense, 5′-CCGGAATTGCTATGTCTCTGGGACACTCGAGTGTCCCAGAGACATAGCAATTTTTTTG-3′; antisense, 5′-AATTCAAAAAAATTGCTATGTCTCTGGGACACTCGAGTGTCCCAGAGACATAGCAATT-3′). Lentiviral shRNA constructs against GFP and MCL1 were obtained from W. Hahn. WT *MCL1* and 3A *MCL1* cDNAs were amplified with PCR and subcloned into the BamHI and SalI sites of the pLenti-GFP-Puro construct (Addgene, catalogue number 658-5).

**Antibodies and reagents.** Anti-Myc antibody (catalogue number sc-40), polyclonal anti-HA antibody (SC-805), anti-cyclin A antibody (SC-751), anti-PLK1 antibody (SC-17783), anti-CUL1 antibody (sc-70895), anti-RICTOR antibody (sc-81538), anti-p27 antibody (sc-528), anti-SKP1 antibody (sc-7163), anti-MCL1 antibody (sc-819) and anti-cyclin E antibody (SC-247) were purchased from Santa Cruz Biotechnology. Anti-tubulin antibody (T-5168), polyclonal anti-Flag antibody (F2425), monoclonal anti-Flag antibody (F-3165), anti-β-catenin antibody (C7207), anti-vinculin antibody (V9131), peroxidase-conjugated anti-mouse secondary antibody (A4416) and peroxidase-conjugated anti-rabbit secondary antibody (A4914) were purchased from Sigma. Anti-MCL1 antibody (4572), anti-BCL2 antibody (2872), anti-COX IV antibody (4850), anti-cleaved caspase 3 (Asp175) antibody (9661), anti-cleaved PARP (Asp214) antibody (9541), anti-ERK1/2 antibody (4695), anti-Jun antibody (9162), anti-phospho-GSK3β (Ser9) antibody (9336) and anti-BIM antibody (4582) were purchased from Cell Signaling Technology. Anti-MULE antibody (A300-486A) was purchased from Bethyl. Monoclonal anti-HA antibody (MMS-101P) was purchased from Covance. Anti-RBX1 antibody (RB-069P1) was purchased from NeoMarker. Another anti-MCL1 antibody (559027) was purchased from BD Pharmingen. Anti-GFP antibody (632380) and another anti-CUL1 antibody (32-2400) were purchased from Invitrogen. Anti-CDH1 antibody (CC43) was purchased from Oncogene. Oligofectamine, Lipofectamine and Plus reagents were purchased from Invitrogen. GSK3β inhibitor VIII was purchased from Calbiochem.

**siRNAs.** Human siRNA oligonucleotides directed against *FBW7*, *SKP2*, *CDH1* and *CUL1* have been described previously[6,28,29]. A human siRNA oligonucleotide that can deplete both β-TRCP1 and β-TRCP2 (sense, 5′-AAGUGGAAUUUGUGGAACAUC-3′) was purchased from Dharmacon. Human siRNA oligonucleotides directed against MULE (MULE-A: sense, 5′-CAUGCCGCAAUCCAGACAUAU-3′)[25] and (MULE-B: sense, 5′-AAUUGCUAUGUCUCUGGGACA-3′)[30] have been validated previously and were purchased from Dharmacon. Luciferase GL2 siRNA oligonucleotide was purchased from Dharmacon. siRNA oligonucleotides to deplete endogenous RBX1 (sense, 5′-AACUGUGCCAUCUGCAGGAACAA-3′), CUL1 (sense, 5′-GGUCGCUUCAUAAACAACAUU-3′) and RICTOR (sense, 5′-AAACUUGUGAAGAAUCGUAUCUU-3′) were synthesized by Dharmacon. Cocktailed siRNAs targeting *SKP1* were purchased from Invitrogen (1299003). A GSK3α-depleting siRNA oligonucleotide (6312) and a GSK3α/β-depleting siRNA oligonucleotide (6301) were purchased from Cell Signaling Technology. The GSK3β-depleting siRNA oligonucleotide (51012) was purchased from Ambion. As described previously, siRNA oligonucleotides were transfected into subconfluent cells with Oligofectamine or Lipofectamine 2000 (Invitrogen) according to the manufacturer's instructions[6].

**Cell culture.** Cell culture including synchronization and transfection has been described previously[6,28]. Wild-type and *FBW7*$^{-/-}$ DLD1 cell lines were gifts from B. Vogelstein. Mouse T-ALL cell lines derived from *Tal1*-transgenic mice were gifts from M. A. Kelliher. Human T-ALL cell lines were previously described[2]. Loucy and CMLT1 T-ALL cell lines were obtained from J. Aster. For various assays described below, as indicated in the figure legends, T-ALL cells were cultured in either 0.5% FBS or 10% FBS-containing medium for sorafenib (ALEXIS Biochemicals) or ABT-737 (Symansis) treatment. In the case of combined treatment with both sorafenib and ABT-737, T-ALL cells were maintained in 10% FBS-containing medium. Lentiviral shRNA virus packaging, retrovirus packaging and subsequent infections were performed as described previously[28]. For cell viability assays, cells were plated at 10,000 per well in 96-well plates, and incubated with the appropriate medium containing sorafenib, ABT-737 or DMSO for 48 h. Assays were performed with CellTiter-Glo Luminescent Cell Viability Assay kit (Promega) according to the manufacturer's instructions. For detection of apoptosis, cells treated with various drugs were stained with propidium iodide (Roche) or co-stained with annexin-V–PE and 7-AAD (Annexin V-PE Apoptosis Detection Kit I, BD Bioscience) according to the manufacturer's instructions. Stained cells were sorted with a Dako-Cytomation MoFlo sorter (Dako) at the Dana-Farber Cancer Institute FACS core facility.

**Immunoblotting and immunoprecipitation.** Cells were lysed in EBC buffer (50 mM Tris, pH 8.0, 120 mM NaCl and 0.5% NP-40) supplemented with protease inhibitors (Complete Mini, Roche) and phosphatase inhibitors (phosphatase inhibitor cocktail set I and II, Calbiochem). The protein concentrations of the lysates were measured using the Bradford Protein Assay reagent (Bio-Rad) on a DU 800 spectrophotometer (Beckman Coulter). The lysates were then resolved by SDS–PAGE and immunoblotted with the indicated antibodies. For immunoprecipitation, 800 μg lysates were incubated with the appropriate antibody (1–2 μg) for 3–4 h at 4 °C followed by 1 h incubation with protein-A sepharose beads (GE Healthcare). Immuno-complexes were washed five times with NETN buffer (20 mM Tris, pH 8.0, 100 mM NaCl, 1 mM EDTA and 0.5% NP-40) before being resolved by SDS–PAGE and immunoblotted with the indicated antibodies. Quantification of the immunoblot band intensity was performed with ImageJ software.

**Detection of MCL1 phosphorylation sites *in vivo*.** To map MCL1 phosphorylation status *in vivo*, 293T cells were transfected with HA–MCL1 using the calcium phosphate method. Thirty hours after transfection, 293T cells were treated with 10 μM MG132 for 16 h to block the 26S proteasome pathway before collecting whole-cell lysates for HA–immunoprecipitation. After extensive washing with NETN buffer, the HA–immunoprecipitates were separated by SDS–PAGE and visualized with colloidal Coomassie blue. The band containing MCL1 was excised and treated with dithiothreitol (DTT) to reduce disulphide bonds and iodoacetamide to derivatize cysteine residues. In-gel digestion of the protein was done using trypsin or chymotrypsin. The resultant peptides were extracted from the gel and analysed by nanoscale-microcapillary reversed phase liquid chromatography tandem mass spectrometry (LC–MS/MS). Peptides were separated across a 37-min gradient ranging from 4% to 27% (v/v) acetonitrile in 0.1% (v/v) formic acid in a microcapillary (125 μm × 18 cm) column packed with $C_{18}$ reversed-phase material (Magic C18AQ, 5 μm particles, 200 Å pore size, Michrom Bioresources) and online analysed on the LTQ Orbitrap XL hybrid FTMS (Thermo Scientific). For each cycle, one full MS scan acquired on the Orbitrap at high mass resolution was followed by ten MS/MS spectra on the linear ion trap XL from the ten most abundant ions. MS/MS spectra were searched using the SEQUEST algorithm against a database that was created based on a protein sequence database containing the sequence for MCL1. They were searched for common contaminants, such as human keratin protein with static modification of cysteine carboxymethylation, dynamic modification of methionine oxidation and serine, threonine and tyrosine phosphorylation. All peptide matches were filtered based on mass deviation, tryptic state, XCorr and dCn and confirmed by manual validation. The reliability of site localization of phosphorylation events was evaluated using the Ascore algorithm.

**Real-time RT–PCR analysis.** RNA was extracted using the RNeasy mini kit (Qiagen), and the reverse transcription (RT) reaction was performed using TaqMan Reverse Transcription Reagents (ABI, N808-0234). After mixing the resultant template with *MCL1* (Hs00172036_m1) or *GAPDH* (Hs99999905_m1) primers and TaqMan Fast Universal PCR Master Mix (ABI, 4352042), the real-time RT–PCR was performed with the 7500 Fast Real-time PCR system (ABI). *FBW7* (Hs00217794_m1), *SKP2* (Hs00180634_m1), *BTRC1* (Hs00182707_m1), *MCL1* (Hs00172036_m1) and *GAPDH* (Hs99999905_m1) primers were purchased from ABI.

**Protein degradation analysis.** Cells were transfected with Myc–MCL1 along with HA–FBW7 or Flag–β-TRCP1, and GFP as a negative control, in the presence or absence of HA–GSK3 and/or HA–ERK1. For half-life studies, cycloheximide (20 μg ml$^{-1}$; Sigma) was added to the media 40 h after transfection. At various time points thereafter, cells were lysed, and protein abundances were measured by immunoblotting analysis.

***In vivo* ubiquitylation assay.** Cells were transfected with a plasmid encoding Flag–Ub along with Myc–MCL1 and HA–FBW7 in the presence or absence of HA–GSK3. Thirty-six hours after transfection, cells were treated with the proteasome inhibitor MG132 (30 μM; Calbiochem) for 6 h and then collected. Anti-Myc immunoprecipitates were recovered and immunoblotted with anti-Flag antibody. Alternatively, cells were transfected with His–Ub along with Myc–MCL1 and HA–FBW7 in the presence or absence of HA–GSK3. Thirty-six hours after transfection,

cells were collected, and the lysates were incubated with Ni-NTA matrices (Qiagen) at 4 °C for 12 h in the presence of 8 M urea, pH 7.5. Immobilized proteins were washed five times with 8 M urea, pH 6.3, before being resolved by SDS–PAGE and immunoblotted with anti-Myc antibody.

***In vitro* ubiquitylation assay.** The *in vitro* ubiquitylation assays were performed as described previously[8]. To purify the $SCF^{FBW7}$ E3 ligase complex, 293T cells were transfected with vectors encoding GST–FBW7, HA–CUL1, Myc–SKP1 and Flag–RBX1. The $SCF^{FBW7}$ E3 complexes were purified from the whole-cell lysates using GST–agarose beads. Purified, recombinant GST–MCL1 proteins were incubated with purified $SCF^{FBW7}$ complexes in the presence of purified, recombinant active E1, E2 (UBCH5A and UBCH3), ATP and ubiquitin. The reactions were stopped by the addition of 2× SDS–PAGE sample buffer, and the reaction products were resolved by SDS–PAGE gel and probed with the indicated antibodies.

***In vitro* kinase assay.** GSK3 was purchased from New England Biolabs. The *in vitro* kinase reaction was performed according to the manufacturer's instructions. Briefly, 5 μg indicated GST fusion proteins were incubated with purified active GSK3 in the presence of 5 μCi [$\gamma$-$^{32}$P]ATP and 200 μM cold ATP in the kinase reaction buffer for 20 min. The reaction was stopped by the addition of SDS-containing lysis buffer, the proteins resolved by SDS–PAGE and phosphorylation detected by autoradiography.

**MCL1-binding assays.** Binding to immobilized GST proteins was performed as described previously[28]. Where indicated, the GST–MCL1 proteins were incubated with GSK3 in the presence of ATP for 1 h before the binding assays.

**Subcellular fractionation.** Mitochondrial and cytosolic (S100) fractions were prepared by resuspending HeLa cells in 0.8 ml ice-cold buffer A (250 mM sucrose, 20 mM HEPES, pH 7.4, 10 mM KCl, 1.5 mM $MgCl_2$, 1 mM EDTA, 1 mM EGTA, 1 mM DTT, 17 μg ml$^{-1}$ phenylmethylsulphonyl fluoride, 8 μg ml$^{-1}$ aprotinin, 2 μg ml$^{-1}$ leupeptin). Cells were then passed through an ice-cold cylinder cell homogenizer. Unlysed cells and nuclei were pelleted by a 10 min, 750 *g* spin. The recovered supernatant was spun at 10,000 *g* for 25 min. This pellet was resuspended in buffer A and represents the mitochondrial fraction. The supernatant was spun at 100,000 *g* for 1 h. The supernatant from this final centrifugation represents the S100 (cytosolic) fraction.

**Mice.** Generation of conditional *Fbw7* knockout mice (Lck-Cre/*Fbw7*$^{fl/fl}$ and Mx1-Cre/*Fbw7*$^{fl/fl}$) was described previously[3,4].

***In vivo* imaging.** CMLT1 cells were infected with lentiviral vectors encoding a shRNA directed against MCL1 (shMCL1) or an irrelevant control (shGFP). After selection in 1 μg ml$^{-1}$ puromycin, cells were engineered for *in vivo* imaging by transduction with a retrovirus encoding a fusion of firefly luciferase fused to neomycin phosphotransferase and were then selected with 0.5 mg ml$^{-1}$ G418. After selection, the luciferase activity of each engineered cell line was measured and found to have a similar reading. Subsequently, equal numbers of viable cells (0.5–1 × $10^7$ cells) were injected into NOD SCID *Il2rg*-null mice through the lateral tail vein. Tumour burden was determined using bioluminescence imaging (IVIS Spectrum, Caliper Life Sciences) after intraperitoneal injection of 75 mg kg$^{-1}$ D-luciferin. Total body luminescence was quantified using the Living Image software package (Caliper Life Sciences) and is expressed as photons per second per standardized region of interest (photons s$^{-1}$ ROI$^{-1}$), encompassing the entire mouse. Data are presented as mean ± s.e.m. with statistical significance determined by Student's *t*-test.


27. Popov, N. *et al.* The ubiquitin-specific protease USP28 is required for MYC stability. *Nature Cell Biol.* **9,** 765–774 (2007).
28. Gao, D. *et al.* Phosphorylation by Akt1 promotes cytoplasmic localization of Skp2 and impairs APCCdh1-mediated Skp2 destruction. *Nature Cell Biol.* **11,** 397–408 (2009).
29. Benmaamar, R. & Pagano, M. Involvement of the SCF complex in the control of Cdh1 degradation in S-phase. *Cell Cycle* **4,** 1230–1232 (2005).
30. Chen, D. *et al.* ARF-BP1/Mule is a critical mediator of the ARF tumor suppressor. *Cell* **121,** 1071–1083 (2005).

nature medicine

# UBE4B promotes Hdm2-mediated degradation of the tumor suppressor p53

Hong Wu[1], Scott L Pomeroy[2], Manuel Ferreira[3], Natalia Teider[2], Juliana Mariani[2], Keiichi I Nakayama[4], Shigetsugu Hatakeyama[5], Victor A Tron[6], Linda F Saltibus[7], Leo Spyracopoulos[7] & Roger P Leng[1]

**The *TP53* gene (encoding the p53 tumor suppressor) is rarely mutated, although frequently inactivated, in medulloblastoma and ependymoma. Recent work in mouse models showed that the loss of p53 accelerated the development of medulloblastoma. The mechanism underlying p53 inactivation in human brain tumors is not completely understood. We show that ubiquitination factor E4B (UBE4B), an E3 and E4 ubiquitin ligase, physically interacts with p53 and Hdm2 (also known as Mdm2 in mice). UBE4B promotes p53 polyubiquitination and degradation and inhibits p53-dependent transactivation and apoptosis. Notably, silencing UBE4B expression impairs xenotransplanted tumor growth in a p53-dependent manner and overexpression of UBE4B correlates with decreased expression of p53 in these tumors. We also show that UBE4B overexpression is often associated with amplification of its gene in human brain tumors. Our data indicate that amplification and overexpression of *UBE4B* represent previously undescribed molecular mechanisms of inactivation of p53 in brain tumors.**



The *TP53* tumor suppressor gene is inactivated in more than 50% of all human tumors, and *TP53* mutations are the most frequently observed genetic event in cancer cells. Thus, loss of p53 has a key role in cancer pathogenesis, and the regulation of p53 expression and its stability are essential for maintaining normal cell growth[1–6]. The ubiquitin ligase Mdm2 (mouse double minute 2) is a crucial negative regulator of p53 (refs. 7–11), and polyubiquitin chains are efficiently recognized by the proteasome[12–14]. Notably, Mdm2 mediates monoubiquitination or multiple-monoubiquitination of p53 (refs. 15–18). Mdm2 does not polyubiquitinate p53, which suggests that additional ubiquitin ligases or cofactors are required for Mdm2-mediated p53 polyubiquitination and degradation.

UBE4B is a human homolog of the *Saccharomyces cerevisiae* protein UFD2. Yeast UFD2 is involved in the ubiquitin fusion degradation (UFD) pathway and is encoded by a single-copy gene[19]. Yeast UFD2 is required for enzymatic activity in ubiquitin chain assembly and was the first E4 ubiquitination factor to be discovered[20]. Ubiquitin is an abundant and essential protein that mediates targeted protein degradation in eukaryotes. Ubiquitin-mediated protein degradation is a three-step process involving three enzymes: E1 (ubiquitin-activating enzyme), E2 (ubiquitin-conjugating enzyme), and E3 (ubiquitin protein ligase). A new class of ubiquitination enzyme, E4 (a ubiquitin chain assembly factor), was recently shown to be necessary for the degradation of some proteins via the ubiquitin fusion degradation (UFD) pathway[20]. Mouse Ube4b mediates ubiquitination in combination with E1 and E2, in the absence of other E3 components, by functioning as an E3 ligase *in vitro*[21]. Recently, it was reported that yeast UFD2 can also function as an E3 ubiquitin ligase[22]. E3 ligases often control the ubiquitination of multiple substrates[23]; for example, Ube4b serves as an E3 and/or E4 ligase for ataxin-3 (ref. 24), fasciculation and elongation protein ζ-1 (ref. 25) and the tumor suppressor p73 (ref. 26). Notably, deletion of mouse *Ube4b* results in marked apoptosis and lethality very early in embryonic development[27]; however, the underlying mechanisms for this lethality remain unclear.

In this study, we show that UBE4B physically interacts with p53 and Hdm2 and also negatively regulates the stability and function of p53. Our findings further show that UBE4B is overexpressed in various brain tumors, and that UBE4B expression and p53 status are inversely correlated in these tumors. Our data provide new insight into the mechanisms of p53 inactivation in brain tumors.

## RESULTS

### UBE4B physically interacts with Hdm2 and p53

We identified Ube4b as an Mdm2-interacting protein using the yeast two-hybrid system (data not shown). To determine whether endogenous UBE4B interacts with Hdm2 and p53 in human cells, we prepared extracts from human BJT fibroblast cells[28] and immunoprecipitated them with UBE4B-, Hdm2-, p53- or β-gal–specific antibodies (**Fig. 1a–d**). UBE4B coimmunoprecipitated with both Hdm2 and p53 (**Fig. 1a–c**). In a reciprocal experiment, Hdm2 and p53 also immunoprecipitated with UBE4B (**Fig. 1b–d**). An *in vitro* GST pull-down assay revealed that His-Ube4b bound GST-Mdm2 and

[1]Heritage Medical Research Center, Department of Laboratory Medicine and Pathology, University of Alberta, Edmonton, Alberta, Canada. [2]Department of Neurology, Children's Hospital Boston, Harvard Medical School, Boston, Massachusetts, USA. [3]Department of Neurosurgery, Massachusetts General Hospital, Harvard Medical School, Boston, Massachusetts, USA. [4]Department of Molecular and Cellular Biology, Medical Institute of Bioregulation, Kyushu University, Higashi-ku, Fukuoka, Japan. [5]Department of Molecular Biochemistry, Hokkaido University Graduate School of Medicine, Kita-ku, Sapporo, Japan. [6]Department of Pathology and Molecular Medicine, Queen's University, Kingston, Ontario, Canada. [7]Department of Biochemistry, University of Alberta, Edmonton, Alberta, Canada. Correspondence should be addressed to R.P.L. (rleng@ualberta.ca).

Received 8 April 2009; accepted 30 November 2010; published online 13 February 2011; doi:10.1038/nm.2283

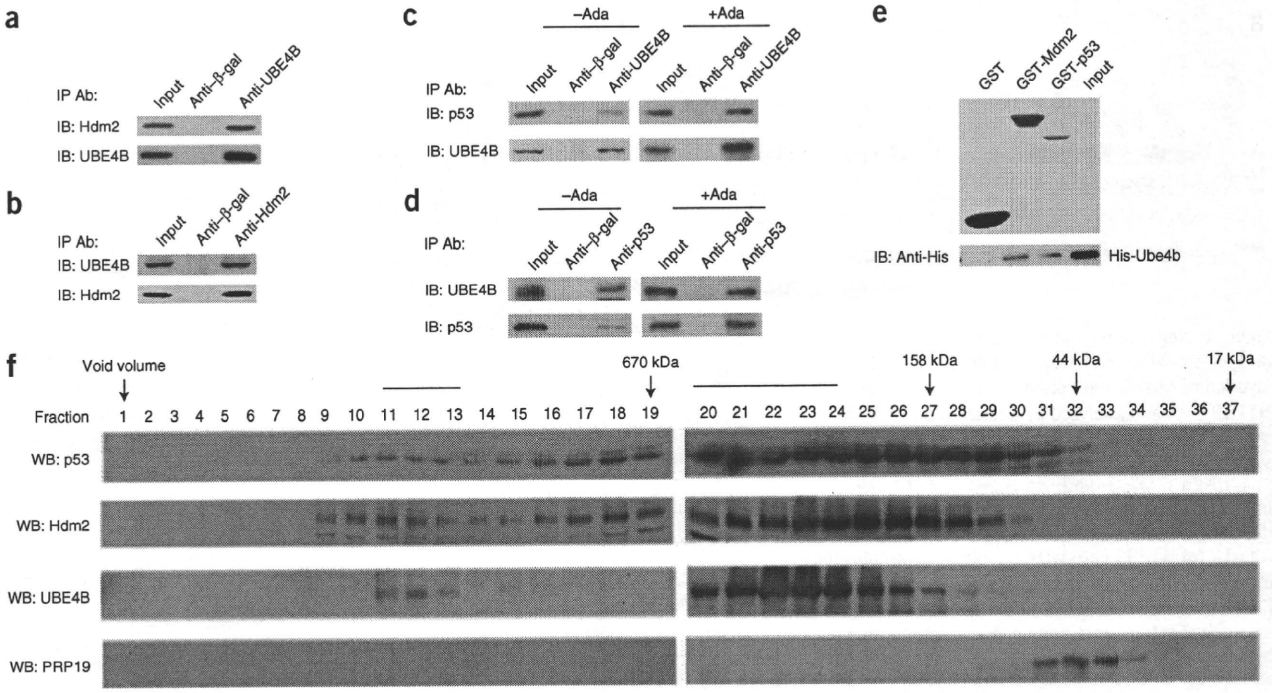


**Figure 1** UBE4B interacts with Hdm2 and p53. (**a**) Western blot with UBE4B-specific or Hdm2-specific (2A10) antibodies after coimmunoprecipitation of Hdm2 from BJT whole cell lysates using UBE4B-specific (UFD2/E4) or β-gal–specific antibodies. (**b**) Western blot with UBE4B-specific and Hdm2-specific (2A10) antibodies after coimmunoprecipitation of UBE4B from BJT whole cell lysates using Hdm2-specific (2A10) or β-gal–specific antibodies. (**c**) Western blot of immunoprecipitates from BJT lysates with p53-specific (DO-1) and UBE4B-specific antibodies. BJT cells were treated with 10 μM of the proteasome inhibitor AdaAhx$_3$L$_3$VS (Ada) for 6 h or mock treated. Total lysates were immunoprecipitated with UBE4B-specific or β-gal–specific antibodies. (**d**) Western blot of BJT lysates with UBE4B-specific and p53-specific (DO-1) antibodies after BJT cells were treated with Ada for 6 h or mock treated. Total lysates were immunoprecipitated with p53-specific (DO-1) or β-gal–specific antibodies. (**e**) The *in vitro* interaction of Ube4b, Mdm2 and p53 was evaluated with GST pull-down assays and western blotting using an antibody against histidine (His-Ube4b). (**f**) BJT cell lysates were subjected to size-exclusion chromatography. Fractions were analyzed by western blotting for the presence of p53, Hdm2, UBE4B and PRP19 (control) with p53-specific (DO-1), Hdm2-specifc (2A10), UBE4B-specific (UFD2/E4) and PRP19-specific antibodies. The elution position of the molecular size markers is shown. In panels **a**–**e** are the eluted proteins probed by antibodies as shown. IB, immunoblot; IP, immunoprecipitation; WB, western blot.



GST-p53, but not GST alone (**Fig. 1e**). The Ube4b-interacting domains mapped to two regions of Mdm2 (amino acids 109–230 and 231–420) and to the amino acids of the DNA-binding domain and the C-terminal region in p53 (**Supplementary Fig. 1a–d**). We then investigated whether UBE4B, Hdm2 and p53 form a complex in cell extracts. BJT cell extracts were fractionated by gel filtration chromatography. We observed one major peak at 606–350 kDa (fractions 20–24), although the elution patterns of p53 and Hdm2 covered a wider range of fractions than that of UBE4B (**Fig. 1f**). In addition, we observed a smaller peak in fractions 11–13. These data indicate that p53, Hdm2 and UBE4B can form a ternary, or higher-order, complex in the cells. We next studied the kinetics of UBE4B or Ube4b induction in human or mouse isogenic pairs of cell lines[28] (**Supplementary Fig. 2a–d**) in response to p53 activation. The increase in UBE4B or Ube4b mRNA or protein was dependent on p53 (**Supplementary Fig. 2a–d**). We further found that the DNA sequences within intron 1 or intron 22 of *Ube4b* contain functional p53 DNA binding sites and are efficiently transactivated by wild-type p53 (**Supplementary Fig. 2e–g**).

### Negative regulation of p53 by Ube4b

Transient overexpression of Ube4b reduced the amount of p53 protein, as did the coexpression of p53 and Mdm2 (**Fig. 2a**). We obtained similar results by overexpression of human UBE4B, Hdm2 and p53 (**Fig. 2b**). In parallel experiments, hemagglutinin (HA)-tagged ubiquitin (HA-Ub) was coexpressed in H1299 cells with plasmids encoding p53 or in combination with Ube4b, or Ube4bΔU (Ube4b in which the U-box has been deleted), or Mdm2, or Mdm2ΔRING, or Ube4b and Mdm2. p53 was immunoprecipitated and analyzed by western blotting with either an HA-specific antibody to detect ubiquitinated p53 (**Fig. 2c**) or a p53-specific antibody (Pab421) to detect total p53 (**Fig. 2c**). The p53 protein (or proteins associated with p53) appeared to be heavily ubiquitinated in the presence of Mdm2 and ubiquitinated to a lesser extent in the presence of Ube4b (**Fig. 2c**). To investigate whether Ube4b, a protein containing a U-box domain, specifically decreases the amount of p53 protein, we tested Ube4b and a number of other U-box–containing proteins for their ability to target p53 for degradation. We found that overexpression of Ube4b, but not of other U-box containing proteins, specifically reduced the amount of p53 protein that could be detected (**Fig. 2d**). To determine whether UBE4B mediates p53 degradation via the ubiquitin-proteasome pathway, we transfected human p53-null H1299 cells with plasmids expressing UBE4B and p53 and treated them with MG132, a proteasome inhibitor. The addition of MG132 greatly increased p53 abundance in the presence of transfected UBE4B compared with the untreated cells, suggesting that UBE4B promotes p53 degradation via the ubiquitin-proteasome pathway (**Fig. 2e**). Immunoprecipitation and western blotting revealed that the immunoprecipitated p53 was either monoubiquitinated or multiple monoubiquitinated in the presence of Hdm2 or polyubiquitinated in the presence of both Hdm2 and UBE4B when the cells were treated with MG132 (**Fig. 2f**).

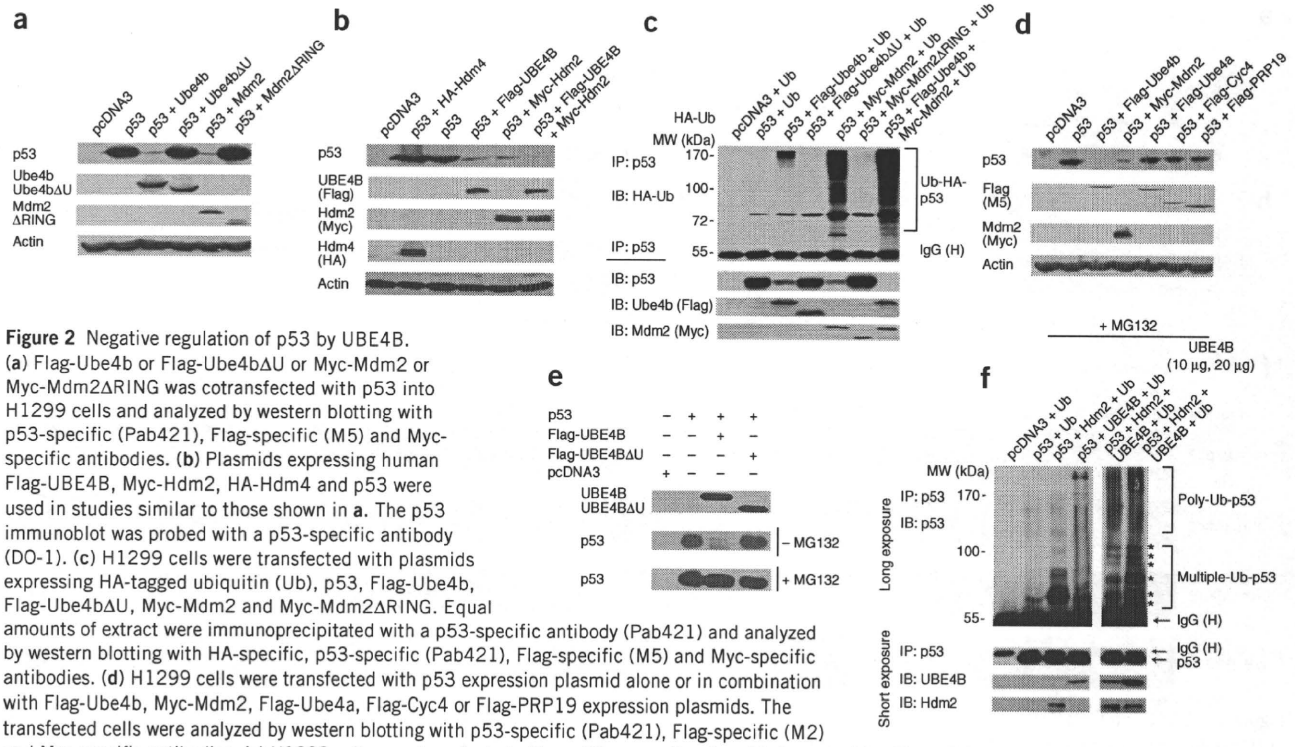


**Figure 2** Negative regulation of p53 by UBE4B. (**a**) Flag-Ube4b or Flag-Ube4bΔU or Myc-Mdm2 or Myc-Mdm2ΔRING was cotransfected with p53 into H1299 cells and analyzed by western blotting with p53-specific (Pab421), Flag-specific (M5) and Myc-specific antibodies. (**b**) Plasmids expressing human Flag-UBE4B, Myc-Hdm2, HA-Hdm4 and p53 were used in studies similar to those shown in **a**. The p53 immunoblot was probed with a p53-specific antibody (DO-1). (**c**) H1299 cells were transfected with plasmids expressing HA-tagged ubiquitin (Ub), p53, Flag-Ube4b, Flag-Ube4bΔU, Myc-Mdm2 and Myc-Mdm2ΔRING. Equal amounts of extract were immunoprecipitated with a p53-specific antibody (Pab421) and analyzed by western blotting with HA-specific, p53-specific (Pab421), Flag-specific (M5) and Myc-specific antibodies. (**d**) H1299 cells were transfected with p53 expression plasmid alone or in combination with Flag-Ube4b, Myc-Mdm2, Flag-Ube4a, Flag-Cyc4 or Flag-PRP19 expression plasmids. The transfected cells were analyzed by western blotting with p53-specific (Pab421), Flag-specific (M2) and Myc-specific antibodies. (**e**) H1299 cells were transfected with a p53 expression plasmid alone or with a Flag-UBE4B or a Flag-UBE4BΔU expression plasmid in the presence or absence of MG132. The transfected cells were analyzed by western blotting with p53-specific (DO-1) or Flag-specific (M5) antibodies. (**f**) Extracts from cells treated with MG132 were immunoprecipitated with a p53-specific antibody (DO-1) and analyzed by western blotting with p53-specific (Ab-7), UBE4B-specific and Hdm2-specific (2A10) antibodies. Asterisks (*) indicate the migration positions of p53-ubiquitin (Ub-p53) conjugates. An antibody to β-actin (actin) was used as a loading control in panels **a–d**. IgG (H), IgG heavy chain.

### Interdependence of UBE4B and Hdm2 in promoting p53 degradation

We tested the ability of UBE4B to regulate endogenous p53 protein in medulloblastoma wild-type p53-expressing H283 cells. The transient overexpression of UBE4B decreased the expression of p53 protein in these cells (**Fig. 3a**). To investigate whether endogenous Ube4b or UBE4B is crucial in regulating the expression level of p53 protein in mouse Neuro2A or human BJT cells, we examined six pairs of both UBE4B-targeting and Ube4b-targeting siRNAs. Two different siRNAs, Ube4b-siRNA1 and Ube4b-siRNA2, effectively knocked down the amount of Ube4b in mouse Neuro2A cells. The decrease in Ube4b was accompanied by an increase in p53 protein and its downstream targets, p21 and Mdm2 (**Fig. 3b**). Notably, a control scrambled siRNA had no effect on the amount of these proteins. We obtained similar results with human BJT cells (**Fig. 3c**).

To determine whether Ube4b promotes p53 degradation through Mdm2, we compared the ubiquitination-promoting activity of ectopically expressed Ube4b and Mdm2 in *Mdm2*$^{-/-}$ *Trp53*$^{-/-}$ mouse embryonic fibroblasts (MEFs). Notably, the overexpression of Ube4b slightly decreased p53 expression when p53 was coexpressed with Ube4b in Mdm2-null MEFs (**Fig. 3d**). In contrast, Ube4b expression greatly reduced the amount of p53 protein in the presence of transfected Mdm2 (**Fig. 3d**). The amount of p53 polyubiquitination was markedly decreased when p53 was coexpressed with Mdm2 in Ube4b-siRNA–treated Mdm2-null MEFs (**Fig. 3e**). We observed a stronger ubiquitinated signal in the presence of Mdm2, Ube4b, or Mdm2 and Ube4b together when the cells were treated with MG132 (**Fig. 3e**). Together, these results suggest that Mdm2 enhances Ube4b-dependent degradation of p53.

To investigate whether Ube4b is required for Mdm2-mediated p53 degradation *in vivo*, we transfected Neuro2A cells with Ube4b-siRNA2 or control siRNA. Two days later, we further transfected these cells with an Mdm2 expression plasmid. Overexpression of Mdm2 did not affect the amount of p53 protein when Ube4b was depleted, suggesting that Ube4b is required for Mdm2-promoted p53 degradation in these cells (**Fig. 3f**). As predicted, the basal level of endogenous p53 protein was also much higher in Ube4b-knockout (*Ube4b*$^{-/-}$) cells than in parental wild-type MEFs (**Fig. 3g**). Consistently, p53 expression was greatly decreased in the presence of transfected Ube4b, and to a lesser extent in either the presence of Ube4b and Ube4bΔU or in the presence of Ube4b alone when Mdm2 was eliminated in Ube4b-knockout MEFs (**Fig. 3h**). These findings suggest that Ube4bΔU may act as a dominant negative to interfere with Ube4b, and that Ube4b promotes p53 degradation that is dependent mainly on Mdm2. We also observed that depletion of Mdm2 did not increase p53 expression in Ube4b-knockout MEFs (**Fig. 3i**). p53 appeared to be heavily ubiquitinated in the presence of Mdm2 in wild-type MEFs, whereas most of these proteins appeared to be monoubiquitinated in Ube4b-knockout MEFs (**Fig. 3j**). However, we still detected >100-kDa p53-ubiquitin conjugates in Ube4b-knockout MEFs that overexpressed Mdm2, suggesting the existence of other molecules capable of targeting p53 for polyubiquitination (**Fig. 3j**). Furthermore, we detected the polyubiquitination of p53 in the presence of transfected Ube4b in Ube4b-knockout MEFs, but not in the presence of Ube4bΔU, suggesting that wild-type Ube4b can restore the function of Ube4b in Ube4b-knockout MEFs, but not Ube4bΔU (**Fig. 3j**). Pirh2 and Cop1 are RING-finger E3 ligases that are involved in the ubiquitination

and degradation of p53 (refs. 28–30). We observed that expression of Pirh2 with Ube4b or Cop1 with Ube4b enhanced the decrease in p53 expression when compared to Pirh2 or Cop1 overexpression alone (**Supplementary Fig. 3a,b**). These findings suggest that Ube4b may also cooperate with Pirh2 and Cop1 to downregulate p53.

The half-life of endogenous p53 in the presence of Ube4b was approximately 10 min ($P < 0.01$, **Supplementary Fig. 4b**), whereas it was approximately 20 min in cells transfected with an empty vector (**Supplementary Fig. 4a**). The half-life of endogenous p53 in the presence of the control siRNA was approximately 19 min; this half-life increased to approximately 32 min in cells depleted of Mdm2 (**Supplementary Fig. 4d**). Furthermore, the ablation of Ube4b increased the p53 half-life to approximately 35 min ($P < 0.05$); the half-life increased to approximately 61 min in cells depleted of both Ube4b and Mdm2 ($P < 0.05$, **Supplementary Fig. 4d**). We also examined the knockdown efficiency of Mdm2 and Ube4b (**Supplementary Fig. 4f**). Together, these data indicate that Ube4b, like Mdm2, regulates the stability of p53 *in vivo*.

### UBE4B shows E4 activity *in vivo* and *in vitro*

To determine whether UBE4B functions as an E3/E4 ligase for p53 *in vivo*, we transfected H283 cells with siRNA constructs targeting specific sequences of UBE4B and, 40 h later, further transfected them with the HA-Ub expression plasmid and immunoprecipitated p53 with a p53-specific antibody (DO-1). Polyubiquitinated p53 abundance was markedly decreased by UBE4B-siRNA treatment when compared to treatment with the control siRNA (**Fig. 4a**). We saw increased polyubiquitination of p53 when the cells were treated with MG132 (**Fig. 4b**). We generated cell lines expressing shRNA against UBE4B (UBE4B-shA) or control-shA cell lines expressing HA-Ub

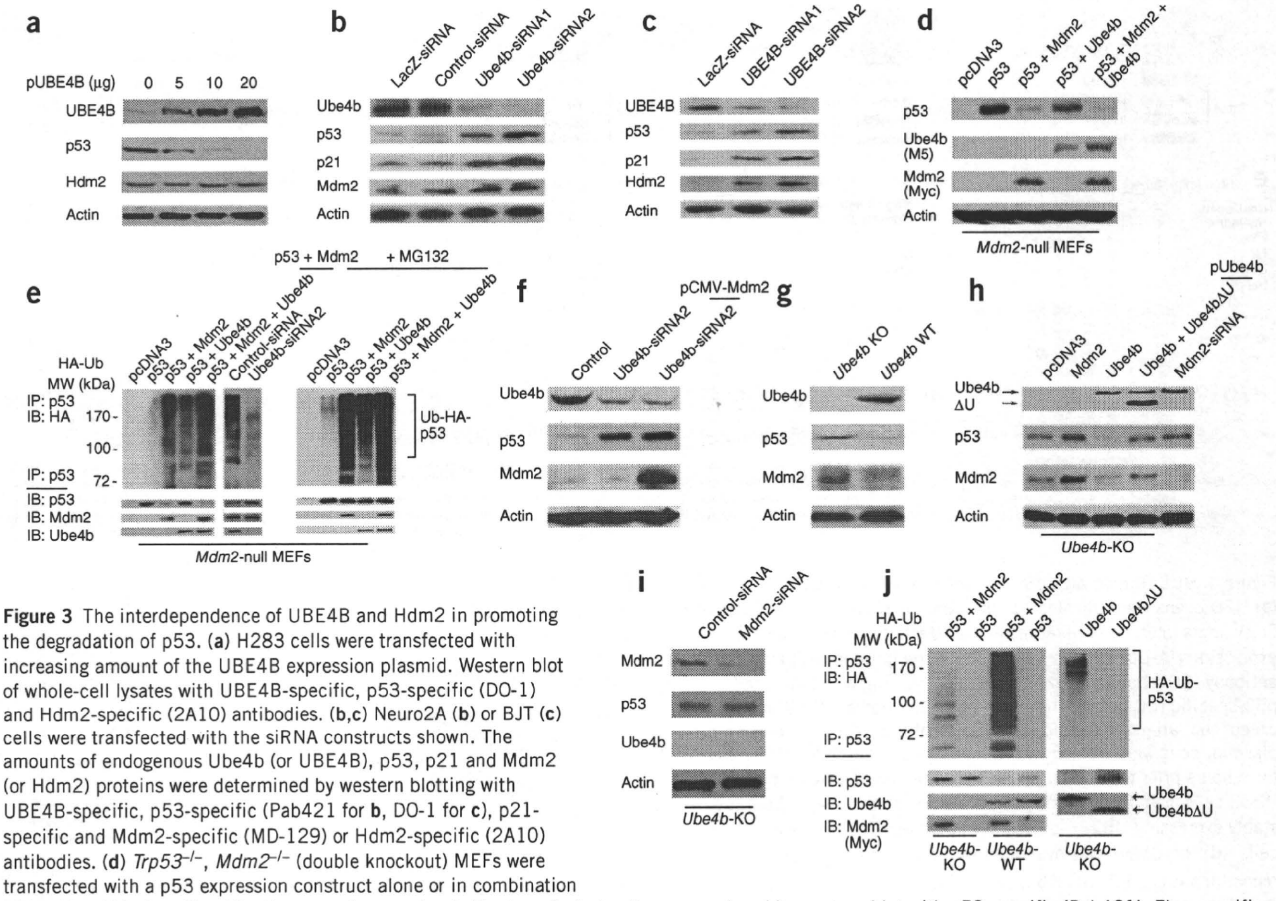


**Figure 3** The interdependence of UBE4B and Hdm2 in promoting the degradation of p53. (**a**) H283 cells were transfected with increasing amount of the UBE4B expression plasmid. Western blot of whole-cell lysates with UBE4B-specific, p53-specific (DO-1) and Hdm2-specific (2A10) antibodies. (**b**,**c**) Neuro2A (**b**) or BJT (**c**) cells were transfected with the siRNA constructs shown. The amounts of endogenous Ube4b (or UBE4B), p53, p21 and Mdm2 (or Hdm2) proteins were determined by western blotting with UBE4B-specific, p53-specific (Pab421 for **b**, DO-1 for **c**), p21-specific and Mdm2-specific (MD-129) or Hdm2-specific (2A10) antibodies. (**d**) *Trp53*$^{-/-}$, *Mdm2*$^{-/-}$ (double knockout) MEFs were transfected with a p53 expression construct alone or in combination with a Myc-Mdm2 or Flag-Ube4b expression construct. The transfected cells were analyzed by western blot with p53-specific (Pab421), Flag-specific (for Ube4b) and Myc-specific (for Mdm2) antibodies. (**e**) Additionally, the extracts from the transfected cells were immunoprecipitated with a p53-specific antibody (Pab421) and analyzed by western blotting with HA-specific or p53-specific (Pab421) antibodies. MG132, a proteasome inhibitor, was added for 6 h before harvest as shown in the right panel. (**f**) Neuro2A cells were transfected with the Ube4b-siRNA2 construct or a control siRNA construct. Thirty hours later, the cells were further transfected with the Mdm2 expression plasmid and analyzed by western blot with Ube4b-specific (UFD2/E4), p53-specific (Pab421) and Mdm2-specific (MD-219) antibodies. (**g**) Cell extracts were prepared from *Ube4b*$^{-/-}$and *Ube4b*$^{+/+}$ MEFs. Western blot analysis of endogenous Ube4b, p53 and Mdm2 proteins with Ube4b-specific (UFD2/E4), p53-specific (CM5) and Mdm2-specific (MD-219) antibodies. (**h**) *Ube4b*$^{-/-}$ (Ube4b KO) MEFs were transfected with the indicated plasmids and analyzed by western blot with Flag-specific (for Ube4b and Ube4bΔU), Mdm2-specific (MD-219) and p53-specific (CM5) antibodies. (**i**) *Ube4b*$^{-/-}$ MEFs were transfected with control-siRNA or Mdm2-siRNA and analyzed by western blot with Mdm2-specific (MD-129), p53-specific (CM5) and Ube4b-specific antibodies. (**j**) *Ube4b*$^{-/-}$ MEFs or wild-type MEFs were cotransfected with plasmids expressing p53, or in combination with Myc-Mdm2, or Flag-Ube4b or Flag-Ube4bΔU as well as HA-Ub. Whole-cell lysates were immunoprecipitated with a p53-specific antibody (Pab421) and analyzed by western blot with HA-specific, p53-specific (Pab421), Flag-specific and Myc-specific antibodies. *Ube4b* KO, *Ube4b*$^{-/-}$ MEFs; *Ube4b* WT, *Ube4b*$^{+/+}$ MEFs. An antibody to β-actin (actin) was used as a loading control in all panels except **e** and **j**.

(**Fig. 4c**). The p53 immunoblot revealed that monoubiquitinated or multiple-monoubiquitinated p53 occurred to a lesser extent in control-shA than in UBE4B-shA cell lines, indicating an inverse correlation between the polyubiquinated and the monoubiquinated forms of p53 (**Fig. 4a–c**). These data show that UBE4B is required for p53 polyubiquitination *in vivo*.

To determine whether p53 could serve as a substrate for Ube4b-dependent ubiquitination *in vitro*, we performed *in vitro* ubiquitination assays[28]. We observed that Ube4b can function as an E3 ligase in promoting protein ubiquitination *in vitro* (**Fig. 4d**). Notably, the p53 immunoblot revealed that either Ube4b or Mdm2 alone promotes only the monoubiquitination of p53 *in vitro* (**Fig. 4d**). To directly test whether the smeared higher-molecular-weight species observed in **Figure 4d** represented polyubiquitinated forms of p53, we performed a coupled *in vitro* ubiquitination-immunoprecipitation. The p53 immunoblot shows that either Ube4b or Mdm2 mediated

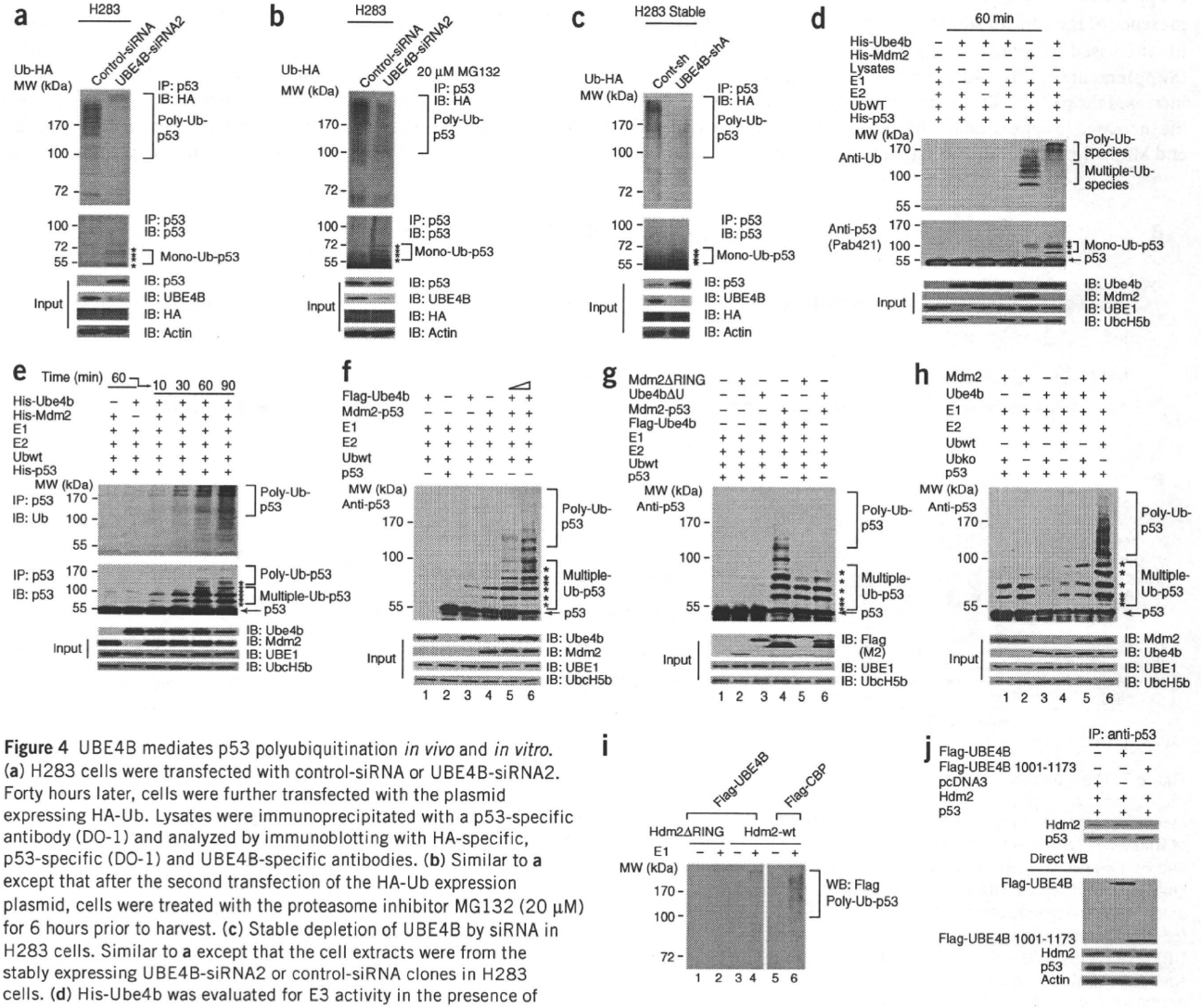


**Figure 4** UBE4B mediates p53 polyubiquitination *in vivo* and *in vitro*. (**a**) H283 cells were transfected with control-siRNA or UBE4B-siRNA2. Forty hours later, cells were further transfected with the plasmid expressing HA-Ub. Lysates were immunoprecipitated with a p53-specific antibody (DO-1) and analyzed by immunoblotting with HA-specific, p53-specific (DO-1) and UBE4B-specific antibodies. (**b**) Similar to **a** except that after the second transfection of the HA-Ub expression plasmid, cells were treated with the proteasome inhibitor MG132 (20 μM) for 6 hours prior to harvest. (**c**) Stable depletion of UBE4B by siRNA in H283 cells. Similar to **a** except that the cell extracts were from the stably expressing UBE4B-siRNA2 or control-siRNA clones in H283 cells. (**d**) His-Ube4b was evaluated for E3 activity in the presence of recombinant E1, E2 (UbcH5b) and ubiquitin. Following the ubiquitination reaction, the samples were analyzed by western blotting with ubiquitin-specific and p53-specific (Pab421) antibodies. Direct western blots for Ube4b, Mdm2, UBE1 and UbcH5b are shown in the lower panel. (**e**) Western blot analysis of a coupled *in vitro* ubiquitination-immunoprecipitation. After the *in vitro* ubiquitination, the samples were immunoprecipitated with a p53-specific antibody (Pab421) and analyzed by western blotting with ubiquitin-specific and p53-specific antibodies. Direct western blots for Ube4b, Mdm2, UBE1 and UbcH5b are shown in the bottom blots. (**f**) Western blot of the *in vitro* ubiquitination reaction probed with a p53-specific (Pab421) antibody. Direct western blots for Ube4b, Mdm2, UBE1 and UbcH5b are shown in the lower panel. (**g**) Western blot similar to **f** except that the copurified Mdm2-p53 complexes were incubated with the purified Ube4bΔU, or the purified Ube4b was incubated with the purified Mdm2ΔRING. (**h**) Western blot of the *in vitro* ubiquitination reaction with a p53-specific antibody (Pab421). Direct western blots for Ube4b and Ube4bΔU (Ube4b polyclonal antibodies[21]), Mdm2 and Mdm2ΔRING (SMP14), UBE1 and UbcH5b are shown in the lower panel. (**i**) Purified HA-p53 was ubiquitinated by Flag-Hdm2 (ref. 31), then immunoprecipitated with HA antibody-conjugated beads to remove Hdm2 and nontagged ubiquitin. The immobilized p53 was then mixed in a second ubiquitination reaction, along with purified Flag-UBE4B and Flag-Ub. Western blot showing HA-p53-conjugates with a Flag-specific antibody (M2). In addition, we added Flag-Hdm2ΔRING as a negative control and Flag-CBP as a positive control. (**j**) U2OS cells were transfected plasmids expressing Flag-UBE4B or Flag-UBE4B 1001-1173. Cell lysates were immunoprecipitated with a p53-specific antibody (FL-393) and analyzed by western blotting with Hdm2-specific (2A10) and p53-specific (DO-1) antibodies. Direct western blot of the samples used is shown in the lower panel. Asterisks (*) indicate the migration positions of p53-ubiquitin conjugates. An antibody to β-actin (actin) was used as a loading control.

monoubiquitination of p53, whereas the combination of the two proteins promoted the polyubiquitination of p53 *in vitro* (**Fig. 4e**). We further confirmed this finding with baculovirus-expressed Mdm2 and Ube4b (**Fig. 4f–h**). The observation of longer chains suggests that Ube4b strongly stimulated the ubiquitination reaction (**Fig. 4f–h**). In addition, there was a dose-dependent increase in the abundance of the high-molecular-weight species of p53; this is consistent with polyubiquitination (**Fig. 4f**)[31]. Moreover, the reaction in the absence of p53 eliminated all p53 signal (**Fig. 4f**). Consistent with this, neither incubation of Mdm2ΔRING (Mdm2 without its RING domain) with Ube4b nor incubation of Ube4bΔU with Mdm2 promoted the polyubiquitination of p53 *in vitro* (**Fig. 4g**). We confirmed that Mdm2 catalyzes p53 monoubiquitination with wild-type ubiquitin or a lysineless ubiquitin mutant, Ubko, that cannot form polyubiquitin chains (**Fig. 4h**). We also found that Mdm2ΔRING or Ube4bΔU partially inhibits Mdm2-mediated or Ube4b-mediated p53 ubiquitination, respectively (**Supplementary Fig. 3c**). Together, these data show that Ube4b functions as an E4 ligase together with Mdm2 to promote p53 polyubiquitination *in vitro*.

To further determine the independent contribution of UBE4B to p53 polyubiquitination, we performed a two-step, *in vitro* E4 assay[31]. We found that UBE4B functions as an E4 ligase for p53 and is dependent mainly on Hdm2 (**Fig. 4i**). However, the E4 ligase function of UBE4B was not absolutely dependent on Hdm2, because we detected a weak signal of poly–Ub-p53 (**Fig. 4i**). Next, we analyzed the effect of UBE4B overexpression on the interaction of Hdm2 and p53. Overexpression of UBE4B reduced the amount of p53, but this did not occur with cells overexpressing UBE4B 1001–1173 (Hdm2 binding-defective mutant) (**Fig. 4j**). Notably, the interaction of Hdm2 and p53 was not substantially changed in the presence of UBE4B. Together, these data indicate that, unlike YY1 (Yin-Yang protein 1)[32], UBE4B is not likely to be required as a molecular clamp for the interaction of Hdm2 and p53.

### UBE4B inhibits p53-dependent transactivation and apoptosis

To investigate the functional consequences of the interaction of UBE4B with p53, we examined the effect of UBE4B expression on p53-mediated transcriptional activation. We found that UBE4B and Hdm2 both repressed p53-dependent transactivation (**Fig. 5a**). Moreover, the UBE4BΔU mutant retained the ability to repress p53-dependent transactivation, suggesting that UBE4B impairs the transactivation function of p53 without targeting it for degradation (**Fig. 5a**). We observed that UBE4B, like Hdm2, can inhibit p53-dependent cell death by long-term colony assays (**Supplementary Fig. 5a,b**). Additionally, we used annexin V staining to determine whether transient UBE4B expression could rescue cells from p53-dependent cell death. The expression of p53 alone resulted in increased apoptosis (**Fig. 5b**). However, the increase in apoptosis could be largely prevented by the coexpression of UBE4B or Hdm2 (**Fig. 5b**). We also discovered that the overexpression of Hdm2 did not rescue cells from p53-mediated cell death when UBE4B was depleted (**Fig. 5c**). The cell cycle arrest that is mediated by p53 is crucial for its tumor suppression function, so we determined whether the inhibition of UBE4B enabled p53 to arrest cells in the G1 phase of the cell cycle. We transfected human BJT fibroblast cells or BJT/DD fibroblast cells (an isogenic derivative expressing the C-terminal fragment of p53 as a dominant-negative p53) with LacZ-siRNA (used as a negative control) or UBE4B-siRNA2. We also examined the knockdown efficiency of UBE4B (**Fig. 5d**). The siRNA-mediated disruption of UBE4B potentiated the ability of p53 to arrest BJT fibroblasts in the G1 phase of the cell cycle (**Fig. 5e**), but this did not occur in the isogenic derivative, BJ/DD (**Fig. 5f**; ref. 28). Together, these data show that UBE4B is involved in the regulation of p53-dependent transactivation and apoptosis as well as in p53-mediated checkpoint control.

### Ube4b promotes tumorigenesis and is elevated in brain tumors

Next, we examined the ability of Ube4b to immortalize primary rat embryonic fibroblasts (REFs). Similar to a previously reported technique for Mdm2 (ref. 33), either Ube4b or Ube4b and an *Hras* (Harvey rat sarcoma virus oncogene) gene were used to generate immortal cell lines (**Supplementary Table 1** and **Supplementary Methods**). We then analyzed the transforming ability of Ube4b by evaluating the cells' capacity for anchorage-independent growth in REFs. The ectopic expression of Ube4b alone did not induce growth in soft agar (**Supplementary Fig. 6a**). However, Ube4b dramatically increased the transformation activity of oncogenic *Hras* in soft-agar colony formation assays (**Supplementary Fig. 6a**), which indicates that Ube4b can cooperate with an activated *Hras* gene to transform primary cells. We found that focus formation was suppressed by p53 in MEFs, which we used because $Trp53^{-/-}$ MEFs are often used for p53 focus formation experiments; $Trp53^{-/-}$ MEFs produced more foci than wild-type MEFs[34,35]. Similar soft agar assays revealed that overexpression of Ube4b in a p53-null background failed to increase the transformation activity of *Hras* (**Supplementary Fig. 6b**). Together, these data indicate that the oncogenic activity of Ube4b is mainly p53 dependent (**Supplementary Fig. 6c**). The combined effects of Ube4b and *Hras* on the transformation of REFs are summarized in **Supplementary Table 1**.

To examine the role of Ube4b in tumor formation *in vivo*, we injected NIH3T3 mouse fibroblast cells expressing an empty vector or vector encoding Ube4bΔU or Ube4b into severe combined immunodeficiency (SCID) mice. SCID mice injected with NIH3T3 cells expressing Ube4b developed large tumors in 3 weeks ($n$ = 10) (**Fig. 6a**). In contrast, NIH3T3 cells expressing Ube4bΔU or an empty vector did not generate any tumors. Given that Ube4b has oncogenic potential, we further examined whether the elimination of Ube4b expression by siRNA could inhibit tumor growth. We used two colorectal cancer cell lines: wild-type human HCT116 (HCT116-WT) and HCT116 $TP53^{-/-}$ (refs. 36,37). SCID mice injected with HCT116-WT cells expressing LacZ-siRNA developed large tumors, whereas mice injected with HCT116-WT cells expressing UBE4B-siRNA developed considerably smaller tumors ($n$ = 10) (**Fig. 6b**). In contrast, HCT116 $TP53^{-/-}$ cells that express UBE4B-siRNA only showed a slight effect on tumor growth compared with cells that express LacZ-siRNA (**Fig. 6b**). We then studied the kinetics of tumor appearance and development in these mice. We found that high Ube4b expression was accompanied by low p53 expression in the Ube4b-expressing tumors (**Fig. 6c**), which suggests that Ube4b induces tumorigenesis by inactivating p53 *in vivo*. As expected, the depletion of UBE4B by siRNA had no effect on p21 protein in HCT116 $TP53^{-/-}$ cells (**Fig. 6d**). In contrast, the decrease in UBE4B expression was accompanied by increased levels of p53 and its downstream target, p21, in HCT116-WT (**Fig. 6e**) but not HCT116 $TP53^{-/-}$ cells (**Fig. 6d**). Together, these data indicate that the overexpression of UBE4B promotes tumor growth and that the elimination of UBE4B is effective in inhibiting growth of p53-expressing tumors.

We next examined whether Ube4b expression is related to the status of p53 in various brain tumors. We found that Ube4b was overexpressed in medulloblastoma tissues derived from $Ptch^{+/-}$ (encoding patched homolog-1) mice (**Fig. 6f**), and UBE4B was overexpressed in human medulloblastoma cell lines (**Fig. 6g**), in human medulloblastoma tissues (**Fig. 6h**), in human ependymoma tissues (**Fig. 6i**) and in human pediatric astrocytoma tissues (**Fig. 6j**). We identified

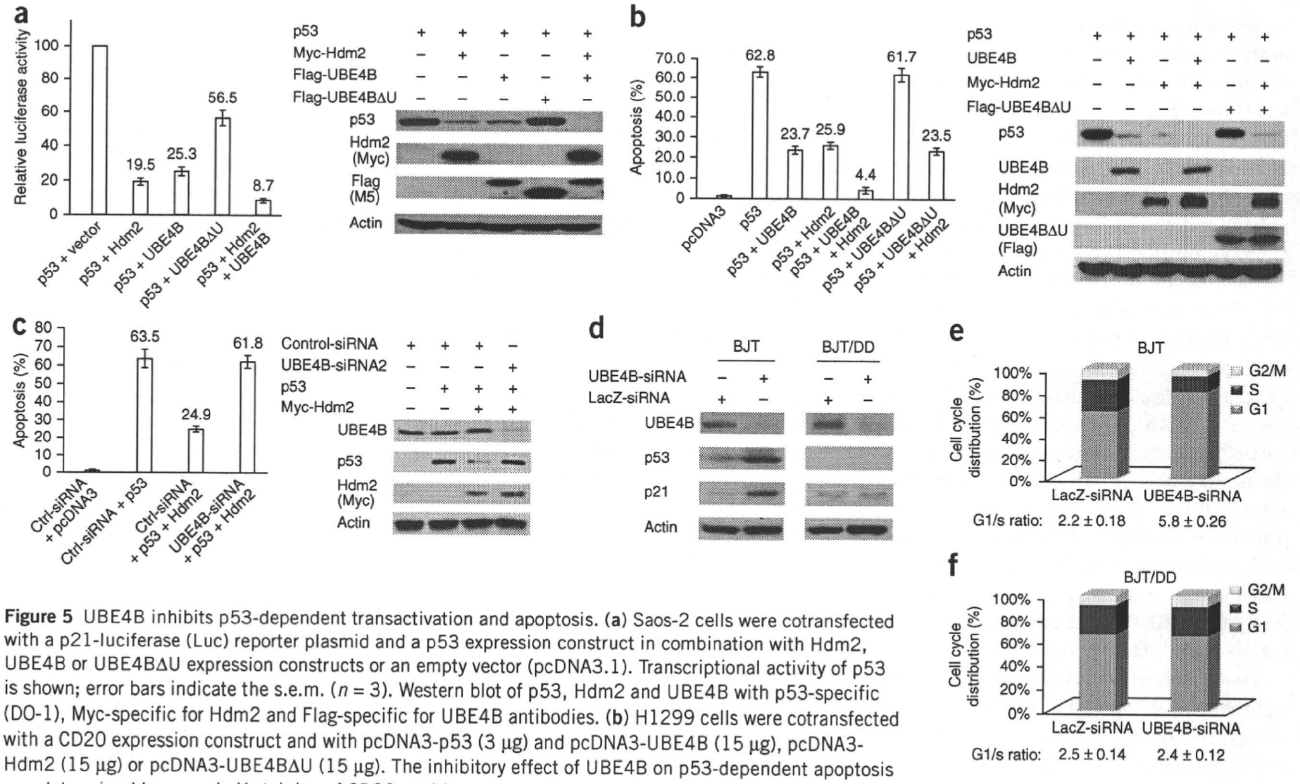


**Figure 5** UBE4B inhibits p53-dependent transactivation and apoptosis. (**a**) Saos-2 cells were cotransfected with a p21-luciferase (Luc) reporter plasmid and a p53 expression construct in combination with Hdm2, UBE4B or UBE4BΔU expression constructs or an empty vector (pcDNA3.1). Transcriptional activity of p53 is shown; error bars indicate the s.e.m. ($n = 3$). Western blot of p53, Hdm2 and UBE4B with p53-specific (DO-1), Myc-specific for Hdm2 and Flag-specific for UBE4B antibodies. (**b**) H1299 cells were cotransfected with a CD20 expression construct and with pcDNA3-p53 (3 μg) and pcDNA3-UBE4B (15 μg), pcDNA3-Hdm2 (15 μg) or pcDNA3-UBE4BΔU (15 μg). The inhibitory effect of UBE4B on p53-dependent apoptosis was determined by annexin V staining of CD20-positive cells and flow cytometry. Error bars indicate the s.e.m. ($n = 3$). Western blot of p53, UBE4B, Hdm2 and UBE4BΔU with p53-specific (DO-1), UBE4B-specific, Myc-specific for Hdm2 and Flag-specific for UBE4BΔU antibodies. (**c**) H1299 cells were transfected with the UBE4B-siRNA or control-siRNA for 30 h. The cells were then transfected with the p53 expression construct alone or in combination with the Hdm2 and CD20 expression plasmids. The number of surviving CD20-positive cells was measured by flow cytometry 24 h after transfection. Error bars indicate the s.e.m. ($n = 3$). Western blot of UBE4B, p53 and Hdm2 with UBE4B-specific, p53-specific (DO-1) and Myc-specific antibodies. (**d**) Depletion of UBE4B by siRNA in BJT and BJT/DD cells, analyzed by western blotting with UBE4B-specific, p53-specific (DO-1) and p21-specific antibodies. (**e**,**f**). BJT (**e**) or BJT/DD (**f**) cells were treated with the LacZ-siRNA or UBE4B-siRNA2, and cell-cycle profile was determined by propidium iodide staining and flow cytometry. G1/s ratio is the ratio of subpopulations and G1-S phase fractions; it indicates the degree of G1 arrest. An antibody to β-actin (actin) was used as a loading control in panels **a**–**d**. Results represent the average of triplicate experiments.

a strong inverse correlation between elevated UBE4B expression and low or undetectable p53 expression ($P < 0.05$, Pearson correlation test). One human ependymoma tissue (NS61) and one pediatric astrocytoma tissue (NS006) had low UBE4B; the two tumor samples had elevated levels of p53 protein (**Fig. 6i,j**). According to mutational analysis, *UBE4B* is infrequently mutated in neuroblastoma and neuroblastoma-derived cell lines[26]. We identified mutations in *TP53* in human medulloblastoma DAOY (elevated p53) and UW228 cell lines, but no mutations of *TP53*, *MDM2* (encoding Hdm2; also known as *Hdm2*) or *UBE4B* in other tumor samples (data not shown). Although we observed upregulation of Hdm2 in some samples with low p53 expression, we detected no substantial *MDM2* gene amplification. These data suggest that Hdm2 is upregulated by mechanisms other than *MDM2* amplification and that p53 stabilization in p53 wild-type tumors may be mediated by the deregulation of UBE4B. Moreover, UBE4B overexpression was inversely correlated with low amount of p53 protein in most of the examined brain tumor samples we analyzed; however, the relationship is not completely reciprocal, because some tumors have decreased UBE4B (**Fig. 6**). Our findings indicate that additional factors may be involved in the formation of these tumors.

To investigate whether gene amplification is a mechanism of UBE4B protein overexpression in brain tumors, we evaluated the copy number of the *UBE4B* gene by real-time quantitative PCR. The *UBE4B* gene was amplified in 44–67% of various types of brain tumors (**Supplementary Fig. 7a–e**). This finding was further confirmed by Southern blot analysis (**Supplementary Fig. 7f–j**). We then used real-time PCR to show that *UBE4B* mRNA was overexpressed in most tumor samples (**Supplementary Fig. 8a–e**). We found a statistically significant relationship between *UBE4B* gene amplification and *UBE4B* mRNA overexpression ($P < 0.05$, Fisher's exact test (two-sided)). Thus, UBE4B overexpression is often associated with its gene amplification.

## DISCUSSION

*TP53* is rarely mutated in medulloblastoma and ependymoma[38,39]. Previous studies have reported that *MDM2* amplification is also uncommon in medulloblastoma and ependymoma[40]. Recent genetic mouse models showed that the loss of p53 accelerates medulloblastoma development[41,42], indicating that the p53 pathway is indeed inactivated in these tumors. However, the mechanism underlying the inactivation of the p53 pathway in brain tumors remains unclear. Mdm2 mediates only the mono- or multiple-monoubiquitination of p53, and it has been proposed that cofactors are required for Mdm2 to promote p53 polyubiquitination and degradation[15–18]. In this study, we report that UBE4B is essential and required for Hdm2-mediated p53 polyubiquitination and degradation.

Mdm2 promotes p53 degradation[7–9], but the mechanisms by which it does so are poorly understood. Here we showed that UBE4B overexpression greatly decreased the amount of p53 protein in various

types of cells and that ablation of UBE4B stabilized the p53 protein. Either Mdm2 or Ube4b alone mediated the monoubiquitination of p53 *in vitro*, while Ube4b, in combination with Mdm2, promoted p53 polyubiquitination *in vitro*. Furthermore, UBE4B can repress p53-dependent transactivation and apoptosis. Elevated UBE4B protein expression has been observed in several brain tumors and various medulloblastoma cell lines (**Fig. 6**). Most notably, we observed an inverse correlation between UBE4B overexpression and low p53 expression in these brain tumors. Our data indicate that amplification and overexpression of *UBE4B* represent a previously undescribed molecular mechanism of inactivation of p53 in brain tumors and that inhibition of UBE4B activity could represent a new approach to the treatment of brain cancer.

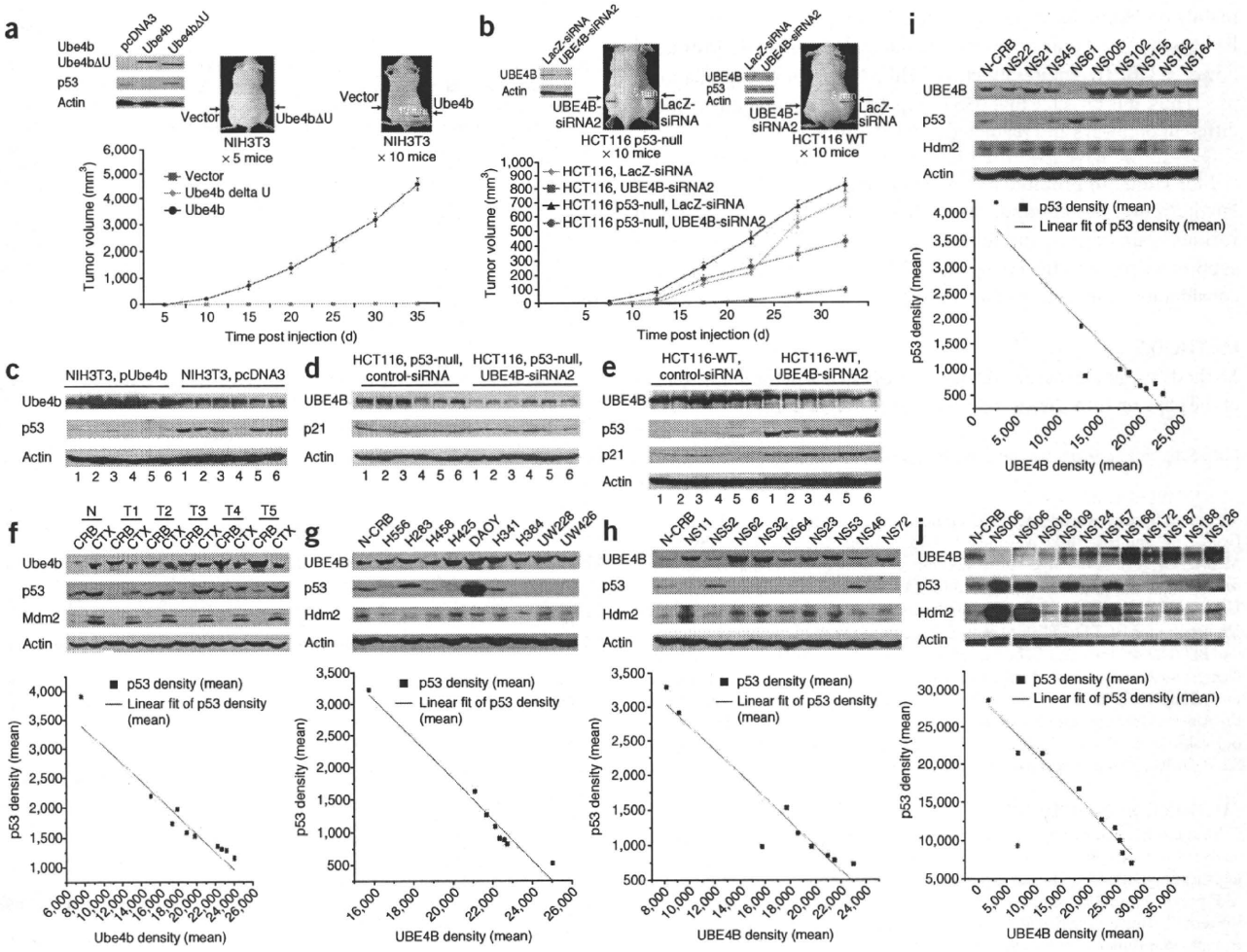


**Figure 6** UBE4B promotes tumorigenesis in a p53-dependent manner and is overexpressed in brain tumors. (**a**) $1 \times 10^7$ NIH3T3 cells expressing Flag-Ube4b or Flag-Ube4bΔU or an empty vector were subcutaneously injected into SCID mice. A portion of the transfected NIH3T3 cells was lysed and analyzed by western blotting as indicated. The tumor volume ($mm^3$) was estimated from caliper measurements. The difference of the population means of the Ube4b-injected group is significantly different compared to the empty vector– and Ube4bΔU-injected groups ($P < 0.01$, one-way ANOVA). Error bars show s.d. ± the mean volume of ten xenografts. (**b**) $1 \times 10^7$ HCT116 *TP53*$^{-/-}$ cells expressing the control siRNA or UBE4B-siRNA2 were subcutaneously injected into SCID mice as indicated (left). A portion of the transfected HCT116 *TP53*$^{-/-}$ cells was lysed and analyzed by western blotting as indicated. Similarly, HCT116-WT cells were used as the tumor cells (right). Tumor size volumes from four different injected groups were analyzed by two-way ANOVA ($P < 0.01$). Error bars show the s.d. from the mean volume of ten xenografts. (**c**–**e**) Six tumor samples from each group mice were dissected 35 d (**c**) or 30 d (**d**,**e**) after injection and analyzed by western blotting with the indicated antibodies. (**f**) Representative western blot analysis of mouse medulloblastoma tissues derived from *Ptch*$^{+/-}$ mice. Proteins were extracted from mouse cerebellum (CRB) and cortex (CTX) and then analyzed by western blotting with indicated antibodies. N denotes normal mouse tissue, and T denotes tumor tissue. The inverse correlation between the amounts of p53 protein that of Ube4b protein was tested with a Pearson correlation test. $y = -0.14881x + 4525.41$; Pearson correlation: −0.96716; significance (two-tailed test): $4.89362 \times 10^{-6}$. (**g**) Whole-cell extracts of medulloblastoma cell lines were analyzed by western blotting with the indicated antibodies. The inverse correlation between the amounts of p53 protein and the amounts of UBE4B protein was tested with a Pearson correlation test. $y = -0.31433x + 8103.88862$; Pearson correlation: −0.98241; significance (two-tailed test): $1.3423 \times 10^{-5}$. (**h**) Similar to **f** and **g** except that proteins were prepared from human medulloblastoma tissues. NS is the prefix for the USA national tissue bank number. The inverse correlation between p53 and UBE4B protein levels was tested with a Pearson correlation test. $y = -0.17304x + 4440.7514$; Pearson correlation: −0.95033; significance (two-tailed test): $8.56558 \times 10^{-5}$. (**i**) Similar to **h** except that proteins were prepared from human ependymoma. The inverse correlation between amount of p53 and UBE4B protein was tested with a Pearson correlation test. $y = -0.17442x + 4192.60377$; Pearson correlation: −0.93287; significance (two-tailed test): $2.41633 \times 10^{-4}$. (**j**) Similar to **h** and **i** except that proteins were prepared from pediatric astrocytoma. The inverse correlation between p53 protein level and UBE4B protein level was tested with a Pearson correlation test. $y = -0.75587x + 29275.47726$; Pearson correlation: −0.98423; significance (two-tailed test): $1.59542 \times 10^{-6}$. An antibody to β-actin (actin) was used as a loading control in panels **c**–**j**.

Recently, YY1, CREB-binding protein (CBP) and E1A binding protein p300 (p300) were reported as E4 ligases that mediate p53 polyubiquitination in humans[17,31,32]. Although CBP is required for p53 polyubiquitination *in vivo*, it shows an Mdm2-independent, p53-directed E4 ligase function[31]. YY1 was described as a molecular clamp to mediate p53 polyubiquitination[32]. In contrast, UBE4B is a U-box–containing E3/E4 ubiquitin ligase. Unlike CBP, UBE4B depends mainly on Hdm2 for its E4 ligase activity for p53. CBP and p300 are E4 ligases and act only on previously monoubiquitinated substrates[31]; however, UBE4B requires functional Hdm2 to promote degradation of p53. Thus, it is possible that p53 is targeted for polyubiquitination by different pathways and regulated through different mechanisms.

Overall, we have identified UBE4B as an E4 ligase that is essential for Hdm2 to promote p53 polyubiquitination and degradation. Furthermore, our findings show that UBE4B is overexpressed in various brain tumors, and they reveal a new link between the tumor suppressor p53 and the oncogene *MDM2*. Thus, these findings have considerable implications for cancer therapy.

## METHODS

Methods and any associated references are available in the online version of the paper at http://www.nature.com/naturemedicine/.

*Note: Supplementary information is available on the Nature Medicine website.*

ACKNOWLEDGMENTS

We gratefully acknowledge W. Gu (Columbia University) for the His-ubiquitin (wild-type) and His-Ub-ko plasmids, A.G. Jochemsen (Erasmus University Medical Center) for the Myc-Mdm2 plasmid, C. Blattner (Universität Heidelberg) for pSuper.neo.gpf-Mdm2 siRNA plasmid, J.A. Mahoney (Johns Hopkins University) for pEF-DEST51-Flag-UBE4B plasmid, B. Vogelstein (Johns Hopkins University) for HCT116 *TP53*$^{-/-}$ cells, S. Benchimol (York University) for BJT and BJT/DD cell lines and G. Lozano (University of Texas, M.D. Anderson Cancer Center) for *Mdm2*$^{-/-}$ *Trp53*$^{-/-}$ MEFs as described in the text. We thank T. Turner for technical help in making the figures. This work was supported by grants from the Alberta Heritage Foundation for Medical Research and Canadian Institutes of Health Research (to R.P.L.) and from the US National Institutes of Health (to S.L.P.). R.P.L. is an Alberta Heritage Foundation for Medical Research scholar.

AUTHOR CONTRIBUTIONS

H.W. and R.P.L. contributed to study design, performed most of the experiments, analyzed and interpreted the data and wrote the manuscript. S.L.P. provided logistical support and all tumor samples and interpreted and discussed the data. M.F. provided technical support and experimental assistance. N.T. conducted the western blotting for the pediatric astrocytoma tissues, isolated genomic DNAs from various tumor samples, carried out mutation detection for p53 in various tumor tissues and medulloblastoma cell lines and did long-term colony assays. J.M. collected tissue samples from various types of human brain tumors, cared for *Ptch*$^{+/-}$ mice, conducted all the mouse genotyping and isolated the cerebellum and cortex from the *Ptch*$^{+/-}$ mice. K.I.N. and S.H. provided the study material and technical support. V.A.T. provided technical support. L.F.S. conducted the FPLC protein purification experiments. L.S. provided technical support for the gel filtration. R.P.L. supervised and directed the project.

COMPETING FINANCIAL INTERESTS

The authors declare no competing financial interests.

Published online at http://www.nature.com/naturemedicine/.
Reprints and permissions information is available online at http://npg.nature.com/reprintsandpermissions/.

1. Farrell, P.J., Allan, G.J., Shanahan, F., Vousden, K.H. & Crook, T. p53 is frequently mutated in Burkitt's lymphoma cell lines. *EMBO J.* **10**, 2879–2887 (1991).
2. Crook, T. & Vousden, K.H. Properties of p53 mutations detected in primary and secondary cervical cancers suggest mechanisms of metastasis and involvement of environmental carcinogens. *EMBO J.* **11**, 3935–3940 (1992).
3. Greenblatt, M.S., Bennet, W.P., Hollstein, M. & Harris, C.C. Mutations in the p53 tumor suppressor gene: Clues to cancer etiology and molecular pathogenesis. *Cancer Res.* **54**, 4855–4878 (1994).
4. Levine, A.J. p53, the cellular gatekeeper for growth and division. *Cell* **88**, 323–331 (1997).
5. Vogelstein, B., Lane, D. & Levine, A.J. Surfing the p53 network. *Nature* **408**, 307–310 (2000).
6. Donehower, L.A. *et al.* Mice deficient for p53 are developmentally normal but susceptible to spontaneous tumours. *Nature* **356**, 215–221 (1992).
7. Haupt, Y., Maya, R., Kazaz, A. & Oren, M. Mdm2 promotes the rapid degradation of p53. *Nature* **387**, 296–299 (1997).
8. Kubbutat, M.H., Jones, S.N. & Vousden, K.H. Regulation of p53 stability by Mdm2. *Nature* **387**, 299–303 (1997).
9. Honda, R., Tanaka, H. & Yasuda, Y. Oncoprotein MDM2 is a ubiquitin ligase E3 for tumor suppressor p53. *FEBS Lett.* **420**, 25–27 (1997).
10. Montes de Oca Luna, R., Wagner, D.S. & Lozano, G. Rescue of early embryonic lethality in mdm2-deficient mice by deletion of p53. *Nature* **378**, 203–206 (1995).
11. Jones, S.N., Roe, A.E., Donehower, L.A. & Bradley, A. Rescue of embryonic lethality in Mdm2-deficient mice by absence of p53. *Nature* **378**, 206–208 (1995).
12. Piotrowski, J. *et al.* Inhibition of the 26 S proteasome by polyubiquitin chains synthesized to have defined lengths. *J. Biol. Chem.* **272**, 23712–23721 (1997).
13. Thrower, J.S., Hoffman, L., Rechsteiner, M. & Pickart, C.M. Recognition of the polyubiquitin proteolytic signal. *EMBO J.* **19**, 94–102 (2000).
14. Pickart, C.M. Ubiquitin in chains. *Trends Biochem. Sci.* **25**, 544–548 (2000).
15. Rodriguez, M.S., Desterro, J.M., Lain, S., Lane, D.P. & Hay, R.T. Multiple C-terminal lysine residues target p53 for ubiquitin-proteasome-mediated degradation. *Mol. Cell. Biol.* **20**, 8458–8467 (2000).
16. Lai, Z. *et al.* Human mdm2 mediates multiple mono-ubiquitination of p53 by a mechanism requiring enzyme isomerization. *J. Biol. Chem.* **276**, 31357–31367 (2001).
17. Grossman, S.R. *et al.* Polyubiquitination of p53 by a ubiquitin ligase activity of p300. *Science* **300**, 342–344 (2003).
18. Li, M. *et al.* Mono- versus polyubiquitination: differential control of p53 fate by Mdm2. *Science* **302**, 1972–1975 (2003).
19. Johnson, E.S., Ma, P.C.M., Ota, I. & Varshavsky, A. A proteolytic pathway that recognizes ubiquitin as a degradation signal. *J. Biol. Chem.* **270**, 17442–17456 (1995).
20. Koegl, M. *et al.* A novel ubiquitination factor, E4, is involved in multiubiquitin chain assembly. *Cell* **96**, 635–644 (1999).
21. Hatakeyama, S., Yada, M., Matsumoto, M., Ishida, N. & Nakayama, K.I. U box proteins as a new family of ubiquitin-protein ligases. *J. Biol. Chem.* **276**, 33111–33120 (2001).
22. Tu, D., Li, W., Ye, Y. & Brunger, A.T. Structure and function of the yeast U-box-containing ubiquitin ligase Ufd2p. *Proc. Natl. Acad. Sci. USA* **104**, 15599–15606 (2007).
23. Koepp, D.M., Harper, J.W. & Elledge, S.J. How the cyclin became a cyclin: regulated proteolysis in the cell cycle. *Cell* **97**, 431–434 (1999).
24. Matsumoto, M. *et al.* Molecular clearance of ataxin-3 is regulated by a mammalian E4. *EMBO J.* **23**, 659–669 (2004).
25. Okumura, F., Hatakeyama, S., Matsumoto, M., Kamura, T. & Nakayama, K.I. Functional regulation of FEZ1 by the U-box–type ubiquitin ligase E4B contributes to neuritogenesis. *J. Biol. Chem.* **279**, 53533–53543 (2004).
26. Hosoda, M. *et al.* UFD2a mediates the proteasomal turnover of p73 without promoting p73 ubiquitination. *Oncogene* **24**, 7156–7169 (2005).
27. Kaneko-Oshikawa, C. *et al.* Mammalian E4 is required for cardiac development and maintenance of the nervous system. *Mol. Cell. Biol.* **25**, 10953–10964 (2005).
28. Leng, R.P. *et al.* Pirh2, a p53 induced ubiquitin-protein ligase, promotes p53 degradation. *Cell* **112**, 779–791 (2003).
29. Sheng, Y. *et al.* Molecular basis of Pirh2-mediated p53 ubiquitylation. *Nat. Struct. Mol. Biol.* **15**, 1334–1342 (2008).
30. Dornan, D. *et al.* The ubiquitin ligase COP1 is a critical negative regulator of p53. *Nature* **429**, 86–92 (2004).
31. Shi, D. *et al.* CBP and p300 are cytoplasmic E4 polyubiquitin ligases for p53. *Proc. Natl. Acad. Sci. USA* **106**, 16275–16280 (2009).
32. Sui, G. *et al.* Yin Yang 1 is a negative regulator of p53. *Cell* **117**, 859–872 (2004).
33. Finlay, C.A. The mdm-2 oncogene can overcome wild-type p53 suppression of transformed cell growth. *Mol. Cell. Biol.* **13**, 301–306 (1993).
34. McCurrach, M.E., Connor, T.M., Knudson, C.M., Korsmeyer, S.J. & Lowe, S.W. bax-deficiency promotes drug resistance and oncogenic transformation by attenuating p53-dependent apoptosis. *Proc. Natl. Acad. Sci. USA* **94**, 2345–2349 (1997).
35. Serrano, M., Lin, A.W., McCurrach, M.E., Beach, D. & Lowe, S.W. Oncogenic *ras* provokes premature cell senescence associated with accumulation of p53 and p16INK4a. *Cell* **88**, 593–602 (1997).
36. Waldman, T. *et al.* Cell-cycle arrest versus cell death in cancer therapy. *Nat. Med.* **3**, 1034–1036 (1997).
37. Bunz, F. *et al.* Requirement for p53 and p21 to sustain $G_2$ arrest after DNA damage. *Science* **282**, 1497–1501 (1998).
38. Saylors, R.L. *et al.* Infrequent p53 gene mutations in medulloblastomas. *Cancer Res.* **51**, 4721–4723 (1991).
39. Gaspar, N. *et al.* p53 Pathway dysfunction in primary childhood ependymomas. *Pediatr. Blood Cancer* **46**, 604–613 (2006).
40. Adesina, A.M., Nalbantoglu, J. & Cavenee, W.K. p53 gene mutation and mdm2 gene amplification are uncommon in medulloblastoma. *Cancer Res.* **54**, 5649–5651 (1994).
41. Crawford, J.R., MacDonald, T.J. & Packer, R.J. Medulloblastoma in childhood: new biological advances. *Lancet Neurol.* **6**, 1073–1085 (2007).
42. Uziel, T. *et al.* The tumor suppressors Ink4c and p53 collaborate independently with Patched to suppress medulloblastoma formation. *Genes Dev.* **19**, 2656–2667 (2005).

## ONLINE METHODS

**Subject data.** All tumor samples were collected at the time of initial diagnosis and before treatment with chemotherapy or radiation in the years 1995–2007 at Children's Hospital Boston. The samples were obtained after informed consent allowing use for the experiments in this study, as approved by the Institutional Review Board of Children's Hospital Boston and Harvard Medical School and the Research Ethics Board of the University of Alberta.

**Plasmids and antibodies.** Ube4b (also called Ufd2a in mouse and UBE4B in humans) or UBE4B or Ube4b mutants were cloned into pcDNA3.1 or p3x Flag-CMV-10 (Sigma-Aldrich), pET28a (Novagen), p21-Luc reporter plasmid described previously[28] or pBacPAK9 (Clontech)[21]. All PCR products were confirmed by sequencing. We used p53-specific antibodies (Pab421, Calbiochem; FL-393, Santa Cruz; DO-1, Abcam; CM5, Novocastra; Ab-7, Oncogene Research Products), Mdm2-specific antibodies (2A10, Calbiochem; SMP14, BD Biosciences; MD-219, Sigma-Aldrich), p21-specific antibody (F-5, Santa Cruz), Myc-tagged–specific antibody (9E10, Roche), Flag-tagged–specific antibodies (M5, M2, Sigma), HA-tagged–specific antibody (12CA5, Roche), ubiquitin-specific, CD20-specific and UFD2/E4-specific antibodies (BD Biosciences), actin-specific antibody (Sigma-Aldrich), PRP19-specific, UBE1-specific and UbcH5b-specific antibodies (Abcam), and polyclonal antibodies for Ube4b (ref. 21).

**Yeast two-hybrid screen.** Yeast strain AH109 was transformed with the plasmid pAS2-1-Mdm2 and a mouse brain cDNA library in the pACT2 vector (Clontech). Approximately $6 \times 10^7$ transformants were screened, and 20 positive clones were isolated after two rounds of growth in the absence of histidine, adenine and screening for β-galactosidase activity. Recovered plasmids from AH109 were used to cotransform Y190 yeast with either full-length Mdm2 or Mdm2 mutants.

**Gel filtration.** Cell lysates were fractioned with a fast protein liquid chromatography protein purification system on a Superose 6 column (GE Healthcare). The column was equilibrated with Tris buffer (50 mM Tris, pH7.5, 150 mM NaCl, 0.1% (vol/vol) Triton X-100), and lysates (2 mg) were applied to and eluted from the column with the same buffer. The flow rate was 0.4 ml $min^{-1}$, and 380 μl fractions were collected. The column was calibrated with Bio-Rad gel filtration standards containing thyroglobulin (670 kDa), γ-globulin (158 kDa), ovalbumin (44 kDa), myoglobin (17 kDa) and Vitamin $B_{12}$ (1.3 kDa).

**siRNA experiments.** We examined six pairs of Ube4b-siRNA. We found that siRNA-2562 (named Ube4b-siRNA1, 5′-CAGCGAGTTCTATGAC AAG-3′) and siRNA-3263 (named Ube4b-siRNA2, 5′-AGAATGCGCGGGCAG AAAT-3′) effectively knocked down endogenous Ube4b. Similarly, we tested six pairs of UBE4B-siRNA and found that the UBE4B-siRNA1 (5′-GCA ACTAGACACCGCGAAA-3′) and UBE4B-siRNA2 (5′-CCCTGTGTGCA ATTTGGTT-3′) effectively knocked down endogenous UBE4B in various human cell lines. pSuper.neo.gfp-Mdm2 siRNA (5′-GACAAAGAAGAGA GTGTGG-3′) was a kind gift from C. Blattner.

**Generation of knockdown cell lines.** The 19-nucleotide oligonucleotides derived from UBE4B-siRNA1, UBE4B-siRNA2, Ube4b-siRNA1 and Ube4b-siRNA2 were cloned into pSuper.puro vector according to the manufacturer's instructions (OligoEngine). To obtain insight into the function of UBE4B or Ube4b, several cell lines were transfected with the plasmids expressing UBE4B-siRNA or Ube4b-siRNA and selected in hygromycine for 2 weeks; thereafter, independent stable clones were selected and evaluated by western blotting.

***In vitro* ubiquitination assay.** The *in vitro* ubiquitination assay was performed as described previously[28]. For the coupled *in vitro* ubiquitination-immunoprecipitation assay, purified His-p53 protein (200 ng) was preincubated with His-Mdm2 protein (200 ng) on ice for 30 min before incubation with ubiquitin reaction components (E1, E2 and ubiquitin). The mixtures were incubated at 30 °C for 30 min to generate ubiquitinated p53. Purified His-Ube4b (300 ng) was then added and followed by additional incubation times, and then the mixtures were immunoprecipitated and analyzed. A One-step E4 assay was done, as described previously[17,31]. Baculovirus-expressed p53 and Flag-Mdm2 were purified as a complex with Flag M2 agarose (Sigma-Aldrich) and then incubated with ubiquitin reaction components at 30 °C for 30 min. Flag-Ube4b was immunopurified from baculovirus-infected sf9 insect cells (Clontech). The Sf9 cell line was derived from pupal ovarian tissue of the fall armyworm *Spodoptera frugiperda*. The Sf9 cell line is highly susceptible to infection with *Autographa california* nuclear polyhedrosis virus (AcNPV baculovirus), and can be used with all baculovirus expression vectors.) was added, followed by further incubation of the reaction at 30 °C for 60 min and analysis by immunoblotting.

***In vivo* ubiquitination assay.** This assay was performed as described previously[28].

**Two–step E4 assay.** This assay was performed as described previously[31]. Briefly, baculovirus-expressed HA-p53 was ubiquitinated by Flag-Hdm2. p53 was immunoprecipitated with beads conjugated with antibody to HA under stringent (RIPA buffer: 50 mM Tris-HCl, pH 7.4; 150 mM NaCl; 0.1% (wt/vol) SDS; 0.5% (wt/vol) Na-deoxycholate; 1% (wt/vol) Nonidet P40) conditions to remove Hdm2 and nontagged ubiquitin. The mixtures were washed three times with RIPA buffer, twice with PBS (137 mM NaCl; 2.7 mM KCl; 10 mM $Na_2HPO_4$; 2 mM $KH_2PO_4$; pH is adjusted to 7.4 with HCl), and twice with Ub buffer (50 mM Tris-HCl, pH 7.4; 2 mM ATP; 5 mM $MgCl_2$; 2 mM DTT). Immunobilized p53 was then mixed with second ubiquitination reaction components (50 ng E1, 100 ng UbcH5b, 5 μg Flag-tagged Ub) along with affinity-purified Flag-UBE4B or Flag-CBP obtained from transfected U2OS (human osteosarcoma; ATCC, HTB-96) cells and incubated at 30 °C for 60 min. To remove UBE4B autoubiquitination products, beads were washed three times with RIPA buffer and then analyzed by western blot with Flag-specific antibodies (M2 or M5, Sigma-Aldrich).

**Xenograft growth assay.** For tumorigenicity assay, $1 \times 10^7$ NIH3T3 cells (ATCC, CRL-1658) expressing Ube4b or Ube4bΔU or empty vector suspended in 0.2 ml HBSS (Invitrogen) were subcutaneously injected into the upper thigh of one or both legs of 6-week-old female SCID mice (Charles River). To examine whether elimination of UBE4B expression by siRNA could inhibit tumor growth, wild-type HCT116 or HCT116 *TP53*$^{-/-}$ cells were transfected with the pSUPER-UBE4B-siRNA2.puro or pSUPER-LacZ-siRNA.puro and selected with 2 μg $ml^{-1}$ puromycin. Independent clones were selected and evaluated by western blotting. The selected clones were allowed to recover in the absence of puromycin. Subsequently, HCT116 or HCT116 *TP53*$^{-/-}$ tumor cells bearing UBE4B-siRNA or LacZ-siRNA were injected into the upper thigh of both legs of 6-week-old female SCID mice. The mice were monitored regularly for tumor growth. Tumor size was measured with a caliper.

**Statistical analyses.** Comparison the half-life of endogenous p53 between overexpressed Ube4b and overexpressed an empty vector or Ube4bΔU was performed with one-way analysis of variance (ANOVA) in OriginLab's Origin Pro 8 software (**Supplementary Fig. 4a–b**). Comparison the half-life of endogenous p53 between siControl and siMdm2 or siUbe4b or siMdm2 and siUbe4b was performed with two-way ANOVA in Origin Pro 8 software (**Supplementary Fig. 4d**). One-way ANOVA in Origin Pro 8 was also used to assess the relationship between Ube4b injected group and the empty vector or Ube4bΔU injected group (**Fig. 6a**). Two-way ANOVA in Origin Pro 8 was also used to assess the tumor size volumes from four different injected groups (**Fig. 6b**). The inverse/negative correlation between UBE4B and p53 protein levels was evaluated statistically by Pearson Correlation Test in Origin Pro 8. In addition, we conducted two-tailed test of significance with the same software (**Fig. 6f–j**). *UBE4B* gene amplification and *UBE4B* mRNA overexpression were calculated by Fisher's exact test (two-sided) in SPSS (PASW) software (**Supplementary Figs. 7a–e** and **8a–e**). The criterion we used to determine statistical significance was $P < 0.05$.

**Additional methods.** Detailed methodology is described in the **Supplementary Methods**.





doi:10.1038/nm.2283